Plate boundary forces are not enough: Second- and third-order stress patterns highlighted in the World Stress Map database

Oliver Heidbach,[1] John Reinecker,[2,3] Mark Tingay,[2,4] Birgit Müller,[2] Blanka Sperner,[2,5] Karl Fuchs,[1,2] and Friedemann Wenzel[1,2]

Received 17 March 2007; revised 3 August 2007; accepted 10 September 2007; published 29 December 2007.

[1] The World Stress Map Project compiles a global database of contemporary tectonic stress information of the Earth's crust. Early releases of the World Stress Map Project demonstrated the existence of first-order (plate-scale) stress fields controlled by plate boundary forces and second-order (regional) stress fields controlled by major intraplate stress sources such as mountain belts and zones of widespread glacial rebound. The 2005 release of the World Stress Map Project database provides, for some areas, high data density that enables us to investigate third-order (local) stress field variations, and the forces controlling them such as active faults, local inclusions, detachment horizons, and density contrasts. These forces act as major controls on the stress field orientations when the magnitudes of the horizontal stresses are close to isotropic. We present and discuss examples for Venezuela, Australia, Romania, Brunei, western Europe, and southern Italy where a substantial increase of data records demonstrates some of the additional factors controlling regional and local stress patterns. **Citation:** Heidbach, O., J. Reinecker, M. Tingay, B. Müller, B. Sperner, K. Fuchs, and F. Wenzel (2007), Plate boundary forces are not enough: Second- and third-order stress patterns highlighted in the World Stress Map database, *Tectonics*, *26*, TC6014, doi:10.1029/2007TC002133.

1. Introduction

[2] The World Stress Map (WSM) is the global compilation of information on the present-day tectonic stress field in the Earth's crust (Figure 1a). The stress information is recorded in a standardized format and quality-ranked in order to be comparable on a global scale [*Sperner et al.*, 2003; *Zoback and Zoback*, 1991; *Zoback*, 1992; *Zoback and Zoback*, 1989]. Over the last 15 years the WSM Project has provided a global database of information on the intraplate state of stress in the Earth's crust [*Heidbach et al.*, 2007; *Sperner et al.*, 2003; *Zoback*, 1992; *Zoback et al.*, 1989]. It has revealed fundamental insights into the first- and second-order patterns of crustal stress on plate-wide and regional scales larger than 500 km as well as on the forces controlling them [*Zoback*, 1992; *Zoback et al.*, 1989] (Figure 1b). The analysis of the first WSM database release in 1992 revealed that the orientation of maximum horizontal compressional stress S_H in North America, South America and Europe are, at the plate scale, predominately subparallel to absolute or relative plate motions [*Müller et al.*, 1992; *Richardson*, 1992; *Zoback*, 1992]. This correlation of stress orientations and plate motions suggests that the first-order intraplate stress patterns are the result of the same forces that drive plate motion, in particular ridge push, slab pull, trench suction, collisional forces, and traction at the base of the lithosphere [*Gölke and Coblentz*, 1996; *Grünthal and Stromeyer*, 1992; *Richardson*, 1992; *Zoback and Zoback*, 1991; *Zoback*, 1992; *Zoback and Burke*, 1993; *Zoback et al.*, 1989]. Second-order stress patterns (100–500 km scales) show that lateral density contrasts, caused by continental rifting, isostatic compensation and topography, deglaciation effects, as well as lithospheric flexure have an additional impact on large-scale stress fields [*Bird et al.*, 2006; *Coblentz et al.*, 1998; *Coblentz and Sandiford*, 1994; *Dyksterhuis et al.*, 2005; *Hillis and Reynolds*, 2000; *Zoback*, 1992; *Zoback and Mooney*, 2003].

[3] The last 20 years have seen a major increase in the application of present-day stress information on smaller spatial scales (<100 km) where third-order effects such as active faults, seismically induced stress changes due to large earthquakes or volcanic eruption, local density contrasts (e.g., from salt diapirs, and detachment horizons) can lead to significant deviations of the stress orientations with respect to the regional and plate-wide stress patterns [e.g., *Bell*, 1996a; *Tingay et al.*, 2006]. These local effects can be key controls for geothermal and petroleum reservoir exploration, production and management [*Fuchs and Müller*, 2001].

[4] Knowledge of the stress field is also critical for seismic hazard assessment [e.g., *Harris et al.*, 1995; *Heidbach and Ben-Avraham*, 2007; *Steacy et al.*, 2005; *Stein et al.*, 1997]. The coseismically induced changes in Coulomb failure stress can serve as indicators for the location and distribution of future earthquakes [e.g., *Harris*, 2002; *Heidbach and*

[1]Geophysical Institute, Universität Karlsruhe (TH), Karlsruhe, Germany.
[2]Heidelberg Academy of Sciences and Humanities, Heidelberg, Germany.
[3]Now at Institute of Geosciences, University of Tübingen, Tubingen, Germany.
[4]Now at School of Earth and Environmental Sciences, University of Adelaide, Adelaide, South Australia, Australia.
[5]Now at Geological Institute, University of Freiberg, Freiberg, Germany.

0278-7407/07/2007TC002133$12.00

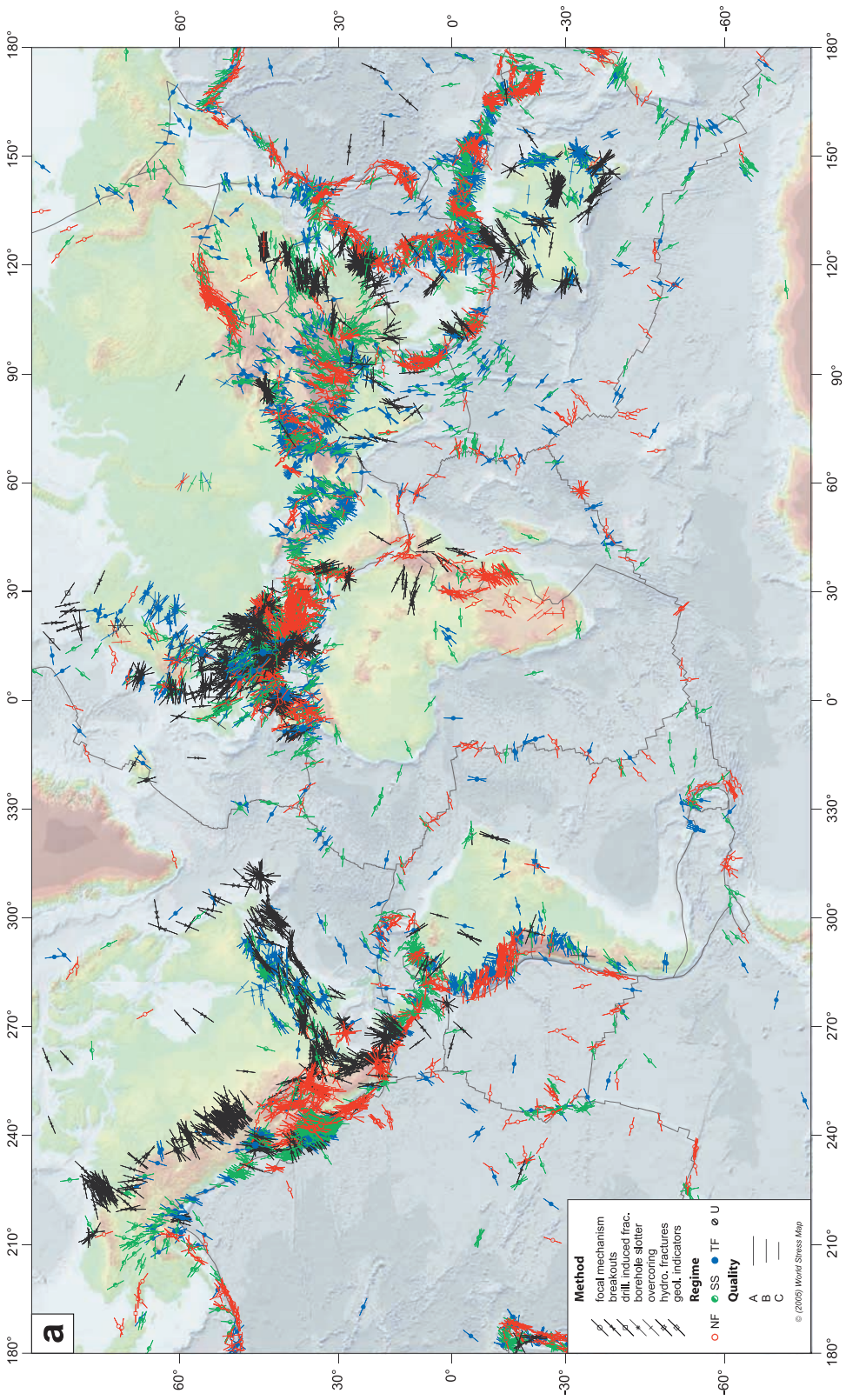
a
Method
focal mechanism
breakouts
drill. induced frac.
borehole slotter
overcoring
hydro. fractures
geol. indicators
Regime
NF SS TF U
Quality
A
B
C
© (2005) World Stress Map

Figure 1a

Ben-Avraham, 2007; *Nalbant et al.*, 2002]. Comparison of stresses before and after strong earthquakes as well as comparison of stress orientations with strain orientations give insights into the amount of coseismic stress drop and local stress changes [*Townend and Zoback*, 2006]. This is associated with changes in the orientation of faults which are optimally oriented with respect to the prevailing regional and local stress field [e.g., *Bohnhoff et al.*, 2006; *Hardebeck and Michael*, 2004; *King et al.*, 1994; *Provost and Houston*, 2003].

[5] For these applications, from plate-wide to regional to local scale, the WSM database provides a fundamental resource. The database itself as well as detailed descriptions for the stress indicators and other database related technical information, are available at the project's web site at http://www.world-stress-map.org. The past WSM releases gave insight into large-scale patterns of regional stress orientations, i.e., the first-order stress patterns due to plate boundary forces, and second-order patterns due to topography, large lateral density variations, and deglaciation effects. However, in addition to further defining broad-scale stress patterns, the WSM 2005 database release has developed some regions of high data density that enables us to investigate variations in stress orientations at local scales and to discuss factors controlling third-order stress patterns. With respect to the WSM 2000 release the WSM 2005 release has increased the number of data records by more than 6600 to a total of almost 16,000 (Figure 1a). The majority of the new data records are from western Europe and areas where basic knowledge on the first- and second-order stress pattern was available before (e.g., California, Australia and in the vicinity of plate boundaries). The intraplate areas of the oceans as well as the continental areas of Africa, Arabia, eastern South America and eastern Europe remain undiscovered in terms of their crustal stress state (Figure 1).

[6] This paper is organized into two sections. In the first, we present major achievements with respect to the last publication on the WSM 2000 database release [*Sperner et al.*, 2003] and give a brief overview on the data types used in the WSM, the quality ranking scheme, and the visualization software tools. Technical changes on the data records of the WSM 2005 database release, the database itself, and the visualization software are documented on the WSM website http://www.world-stress-map.org. In the second section, we illustrate the time and scale dependence of stress patterns by zooming into the stress patterns of western Europe. Furthermore, we present case studies at different spatial scales from Venezuela, Australia, Romania, and Brunei where the increase in data records gave new detailed insights into regional to local stress field properties and thus enabled new tectonic interpretations.

2. WSM Database

[7] The WSM project is a collaborative project of academia, industry and governmental organizations that aims to understand the sources of stress in the Earth's crust. It was initiated in 1986 under the auspices of the International Lithosphere Program. The results of the first WSM compilation were published in 1992 [*Zoback*, 1992]. Since 1995 the WSM is a research project of the Heidelberg Academy of Sciences and Humanities and is located at the Geophysical Institute of Universität Karlsruhe (TH) in Germany.

[8] Updates of the WSM database have been made available online in 1997, 2000, 2003, 2004, and in December 2005 (B. Müller et al., 2000 and 1997 releases of the World Stress Map, and J. Reinecker et al., 2003, 2004, and 2005 releases of the World Stress Map, available online at www.world-stress-map.org) [*Sperner et al.*, 2003]. The total number of data records increased from ~7300 in 1992 over 10,920 in 2000 to 15,969 data records in 2005.

2.1. Data Types

[9] The present-day stress orientation is deduced from focal mechanisms (FM), borehole breakouts (BO), drilling-induced fractures (DIF, from borehole images or caliper log data), in situ stress measurements (OV: overcoring, HF: hydraulic fracturing, BS: borehole slotter), and geological indicators (GF: fault slip data, GVA: volcanic vent alignments). Further details on each method are given by *Zoback and Zoback* [1989, 1991], *Zoback* [1992], *Zoback and Zoback* [2002], *Sperner et al.* [2003], *Wagner et al.* [2004], *Bell* [1996b], and references therein.

[10] The various stress indicators reflect the stress field of different rock volumes ranging from 10^{-3} to 10^{9} m^3 [*Ljunggren et al.*, 2003] and different depths ranging from near surface down to 40 km depth. Within the upper 6 km of the Earth's crust the stress field is mapped by a wide range of methods with borehole breakouts as a major contributor. Below ~6 km depth focal mechanisms are the only stress indicators available, except a few scientific drilling projects such as the KTB project in Germany which reached a depth of 9.1 km [*Brudy et al.*, 1997].

2.2. Quality Ranking Scheme

[11] The success of the WSM is based on a standardized quality ranking scheme for the individual stress indicators making them comparable on a global scale. The quality

Figure 1a. Distribution of stress data records with A-C quality. Colors indicate stress regimes with red for normal faulting (NF), green for strike-slip faulting (SS), blue for thrust faulting (TF), and black for unknown regime (U). Lines represent the orientation of maximum horizontal compressional stress (S_H); line length is proportional to quality. Plate boundaries are taken from the global model PB2002 of *Bird* [2003]. Topography is based on the ETOPO2 data from the National Geophysical Data Center (NGDC) including bathymetry data of *Smith and Sandwell* [1997].

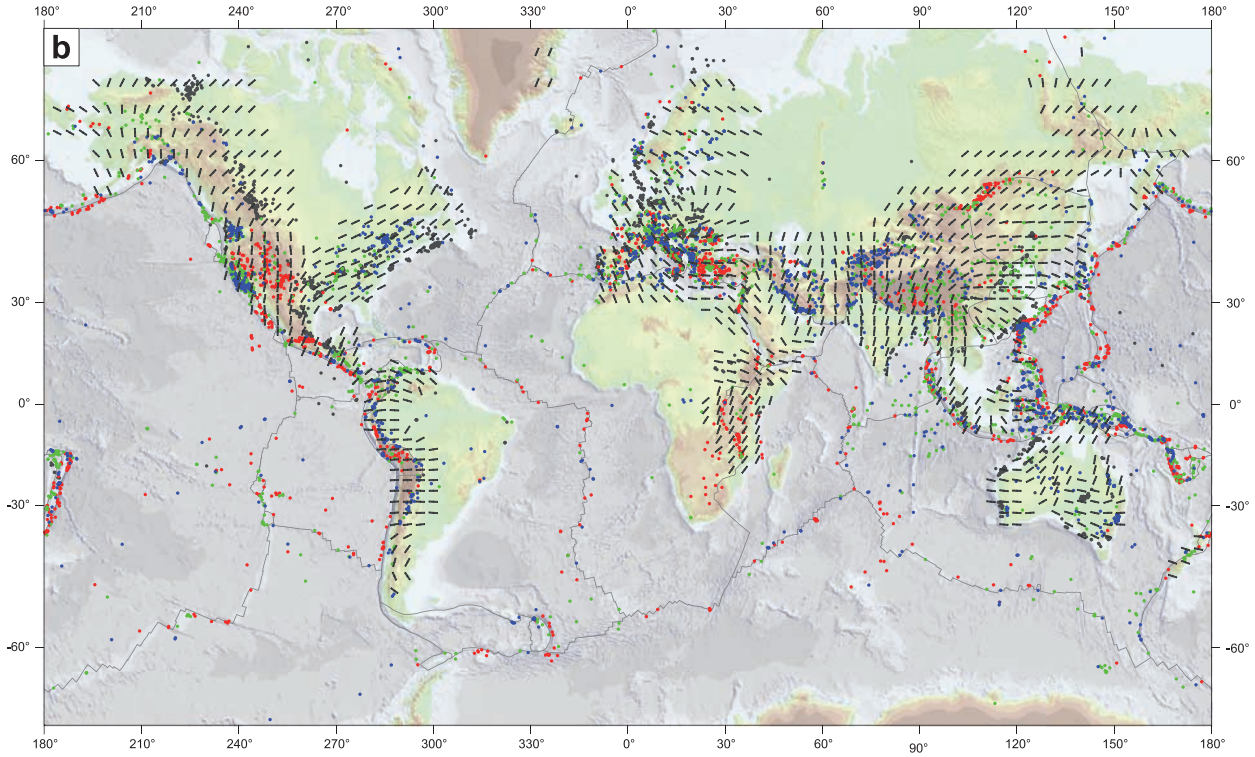

Figure 1b. Legend, stress symbols, and data as in Figure 1a. Thick grey lines represent the smoothed stress field for continental areas using a quality- and distance-weighted algorithm [*Müller et al.*, 2003]. The search radius is r = 750 km, and a minimum of 10 data records within the search radius is requested for calculating the mean stress orientation at a grid point. Note the plate-wide stress pattern and the correlation between the changes from strike-slip and thrust faulting toward normal faulting in areas with high topography.

ranking scheme was introduced by *Zoback and Zoback* [1989, 1991], and refined and extended in the work of *Sperner et al.* [2003]. Details on the quality ranking scheme can be found on the project's web site at http://www.world-stress-map.org. It is internationally accepted and guarantees reliability and global comparability of the stress data. Each stress data record is assigned a quality between A and E, with A being the highest quality and E the lowest. A-quality means that the orientation of the maximum horizontal compressional stress (S_H) is accurate to within ±15°, B-quality to within ±20°, C-quality to within ±25°, and D-quality to within ±40°. For most methods these quality classes are defined through standard deviation of S_H. E-quality data records do not provide sufficient information or have standard deviations greater than 40°. These data records, mainly from well bores containing insufficient stress information, are only kept for bookkeeping purposes. In general, A-, B- and C-quality stress indicators are considered reliable for the use in analyzing stress patterns and the interpretation of geodynamic processes.

2.3. Stress Information

[12] All stress information is compiled in a database of standardized format. The minimum information for each stress data record is the orientation of S_H, the quality of the S_H orientation, the type of stress indicator, the location and depth of the measurement, the tectonic stress regime, and the source references. Additional information is compiled according to the different types of stress indicators such as stress magnitude, number of measurements, rock parameters, and rock age.

2.4. Database Access and Visualization

[13] The database can be downloaded from the WSM web site (www.world-stress-map.org) in three different data formats: ASCII, MS Excel®, and dBase®. In order to visualize the data records stress maps showing the S_H orientation, the quality, the type of stress indicator, and the stress regime can be used (Figure 1a). The project's web site provides 65 predefined stress maps for selected regions worldwide. In addition, users can generate their own custom-made stress maps either by using the Web-based database interface CASMO (Create A Stress Map Online), available at http://www.world-stress-map.org/casmo [*Heidbach et al.*, 2004] or the offline software CASMI (Create A Stress Map Interactively) [*Heidbach and Höhne*, 2007]. CASMI is a public domain program running under Unix-like operating systems. It has a graphical user interface based on the public domain software GMT (Generic Mapping Tools) [*Wessel and Smith*, 1998] and with specific

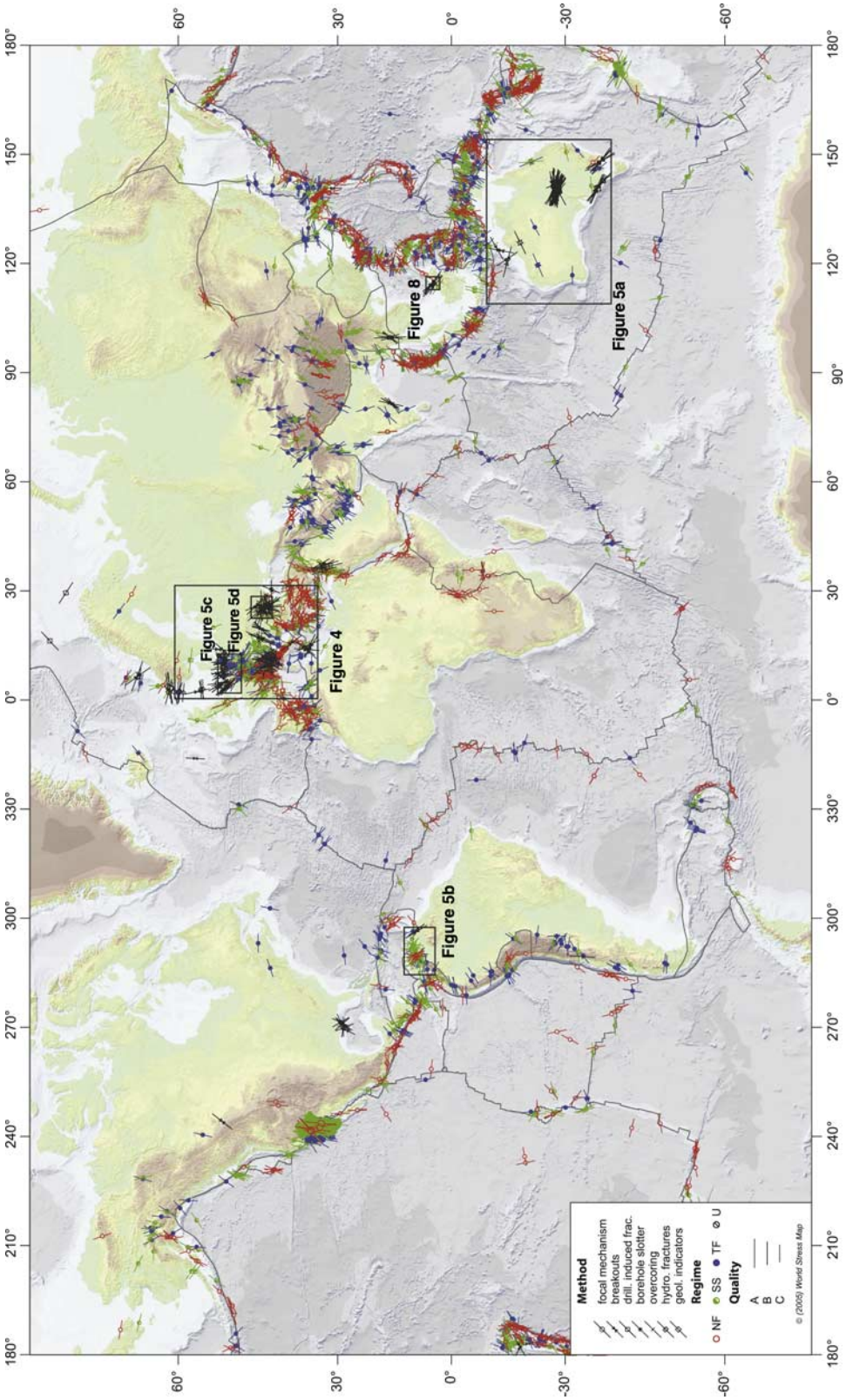

Figure 2. Global distribution of new data records with A-C quality since the WSM database release 2000. Boxes indicate location of stress map examples given in Figures 5a–5d and Figures 4 and 8. Stress symbols are as in Figure 1.

Table 1. Data Type and Quality Distribution in the WSM 2005 Database Release and Increases Since 2000

Data Type (Abbreviation)	WSM 2005 A-E Quality	WSM 2005 A-C Quality	Increase Since 2000 A-E Quality[a]	Increase Since 2000 A-C Quality[a]
Focal mechanisms (FMS, FMC, FMA)	10,619	9278	5067	4882
Borehole breakouts (BO, BOC, BOT)	3365	1905	1056	264
Drilling-induced fractures (DIF)	248	76	203	40
Geological: fault slip (GFI, GFM, GFS)	434	358	108	73
HydroFrac (HF, HFG, HFP, HFM)	349	228	89	70
Borehole slotter (BS)	33	0	33	0
Overcoring (OC)	611	94	16	4
Geological: volcanic alignment (GVA)	220	98	7	7
Petal centreline fractures (PC)	9	9	0	0
Shear wave splitting (SW)	2	0	0	0
Stress indicator not given (none)[b]	79	0	79	0
Total	15,969	12,046	6658	5340

[a]Column gives the total number of new data. However, the difference with respect to the total number given in the first column will not result in the number of data in the WSM 2000 release of *Sperner et al.* [2003] since data eliminated from the database are not taken into account.
[b]These are data records with E-quality from well bores where the data type is unknown.

features needed to visualize the WSM data. CASMI includes the WSM 2005 database release and will be sent free of charge after registration at the project's web site (http://www.world-stress-map.org/casmi).

2.5. Achievements of the WSM 2005 Database Release

[14] The WSM 2005 database release has, in comparison to the WSM 2000 release, 6658 new or revised data records, respectively (Figure 2). From the total number of 15,969 data records more than 12,000 data records are assigned to A-, B-, or C-quality (Figure 1), i.e., they are considered to show the S_H orientation to within ±25° (Table 1 and Figure 3a). Most of the stress data records were derived from earthquake focal mechanisms (77%) and borehole breakouts (16%, Figure 3b). The majority of the new and revised data records are deduced from focal mechanism solutions (76%), borehole breakouts (16%), and drilling-induced fractures (3%). Approximately 80% of these new data records have A- to C-quality (Table 1). Most of the stress data records deduced from focal mechanisms are taken from the Global CMT Project (formally known as Harvard CMT catalogue; now available online under www.globalcmt.org), and published since 1983 in a series of reports in *Physics of the Earth and Planetary Interiors* [e.g., *Ekström et al.*, 2005]. The tectonic stress regime could be assigned for 83% of the A-C quality data (Figure 3c). For the remaining 17% of data records the stress regime is unknown, either because this information is in most cases not available for borehole breakouts and drilling-induced fractures, or because the principal axes are too oblique to the Earth's surface.

3. Scale-Dependent Stress Patterns

[15] The increase of present-day stress data records in the WSM 2005 database release provides a detailed stress data set in a number of regions. Zooming into local scales, i.e., regions with lateral extent in the order of the crustal thickness or smaller, we can now clearly identify stress rotations with respect to the plate-wide and regional stress orientation due to third-order sources of stress. Seven examples with stress patterns from different spatial scales are presented in the following sections. We discuss these examples in decreasing spatial scales, from plate-wide via regional to local scales.

3.1. Plate-Wide Stress Pattern: Impact of Plate Boundary Forces

3.1.1. Stress Map of Western Europe

[16] For western Europe the WSM 2005 database release provides 3188 data records with 1811 of these having A-C quality (Figure 4). According to the principal findings of *Müller et al.* [1992], the first-order pattern shows a prevailing NW to NNW orientation of S_H. *Müller et al.* [1992] conclude from their analysis that this orientation is mainly controlled by plate boundary forces, in particular by ridge push of the North Atlantic and collision of the Africa Plate with the Eurasia Plate. This has been confirmed by several large-scale finite element models [*Gölke and Coblentz*, 1996; *Grünthal and Stromeyer*, 1992, 1994; *Jarosinski et al.*, 2006]. Even though the amount of stress data for western Europe has almost doubled since 1992, this first-order pattern is still clearly visible in the smoothed stress field (Figure 4). The prevailing S_H orientation is parallel to the relative plate motion of the Africa Plate with respect to the Eurasia Plate. Large-scale deviations from this trend occur in the Aegean and the western Anatolian region, where the slab rollback at the Hellenic arc induces a E-W S_H orientation in the back-arc region [*Heidbach and Drewes*, 2003], and in the Pannonian Basin where the NE-SW orientation of S_H is probably due to collision in the Dinarides [*Bada et al.*, 1998, 2007].

[17] The smoothed S_H orientation across Italy is similar to that in western Europe (Figure 4). It shows a NW-SE trend indicating that the convergence between the Africa Plate and the Eurasia Plate is responsible for this large-scale stress field. Local deviations near the coast and toward the Alps and Dinarides might result from lateral density contrasts, topography, the ongoing counterclockwise rotation of the Adriatic Block relative to the Eurasia Plate, and the

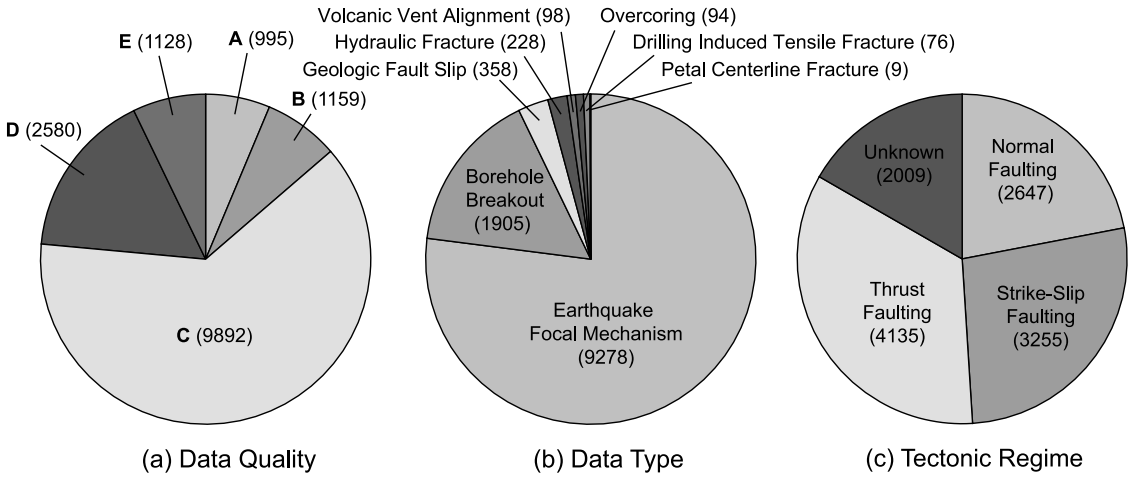

Figure 3. Distribution of data records according to (a) data quality (n = 15,969) (b) data type (only A-C, n = 12,046), and (c) tectonic stress regime (only A-C, n = 12,046). Number of data records is given in brackets.

collisional resistance along the NW-SE striking Dinaride mountains.

[18] Plate boundary forces are clearly identified as the key control for the western European first-order plate-wide stress pattern as well as for other large tectonic plates such as the South America Plate [*Assumpção*, 1992; *Coblentz and Richardson*, 1996; *Meijer et al.*, 1997; *Meijer and Wortel*, 1992] and the North America Plate [*Humphreys and Coblentz*, 2007; *Richardson and Reding*, 1991; *Zoback and Zoback*, 1991; *Zoback*, 1992; *Zoback and Zoback*, 1989]. However, the reverse statement, i.e., that plate boundary forces do not control the stress pattern in areas not exhibiting large-scale stress patterns, is not always true, as demonstrated by the stress field across the Australian continent, shown in the next example.

3.1.2. Stress Map of Australia

[19] The data compilation for Australia and neighboring countries has been accomplished by the research team of the Australasian Stress Map (ASM) Project [*Hillis and Reynolds*, 2000] following the WSM quality assessment scheme. The ASM now contains almost 1000 A-C quality stress data records [e.g., *Hillis et al.*, 1999, 1997; *Hillis and Reynolds*, 2000; *Reynolds and Hillis*, 2000]. The Australian stress pattern is more diverse than the one from western Europe, North America or South America on the same spatial scale. Although the Australian continent is moving roughly NNW, it exhibits a number of distinct stress provinces with different mean S_H orientations [*Hillis and Reynolds*, 2000; *Reynolds et al.*, 2002]. Whereas southwestern Australia has a prevailing E-W S_H orientation, northern Australia has a NE-SW to N-S trend, and in southeastern Australia the mean S_H orientations range from NW-SE over E-W to SW-NE (Figure 5a). Thus the correlation of plate motion trajectories with S_H orientations is not visible [*Hillis and Reynolds*, 2000; *Zoback*, 1992; *Zoback et al.*, 1989]. However, despite this lack of an apparent link between the present-day stress and plate motion, the present-day stress field across Australia is still primarily controlled by far-field forces exerted at the plate boundary.

[20] In contrast to other large continental plates the Indo-Australia Plate is bordered by a complex pattern of different plate boundary types causing the diversity in the large-scale stress pattern [*Hillis and Reynolds*, 2000]. Even though the southern plate boundary exclusively consists of oceanic rifting, the northern, northwestern and eastern plate boundaries show a wide range of convergent and transform plate boundaries alternating on small scales [*Bird*, 2003]. In particular, the Indo-Australia Plate exhibits well defined stress fields, oriented normal to the plate boundary, that radiate outward from zones of continental collision, such as the Himalayas, Papua New Guinea and New Zealand (Figure 1). Furthermore, at the northern border the ongoing collision of the Ontong-Java Plateau with the Indo-Australia Plate causes a complex situation including subduction with different orientations, rollback of subduction zones which impose suction forces, back-arc spreading, and oceanic collision [*Bird*, 2003; *Mann and Taira*, 2004]. Also, farther west the distribution and orientation of different plate boundary forces is complex [*Bird*, 2003]. However, even though the stress pattern in the Indo-Australia Plate is diverse, plate boundary forces are controlling the S_H orientation [*Hillis and Reynolds*, 2000]. This is confirmed by numerical finite element studies of *Coblentz et al.* [1998], *Reynolds et al.* [2002], *Sandiford et al.* [2004], and *Dyksterhuis et al.* [2005]. These models show that the diversity of stress patterns in Australia monitors the complexities of the plate boundary geometry of the Indo-Australia Plate. The comparatively simple absolute motion-parallel plate-scale stress patterns in the Eurasia, the North America, and the South America Plate are (tectonically) bordered by rather simple boundary geometries with forces pushing and pulling the plate in broadly the same direction.

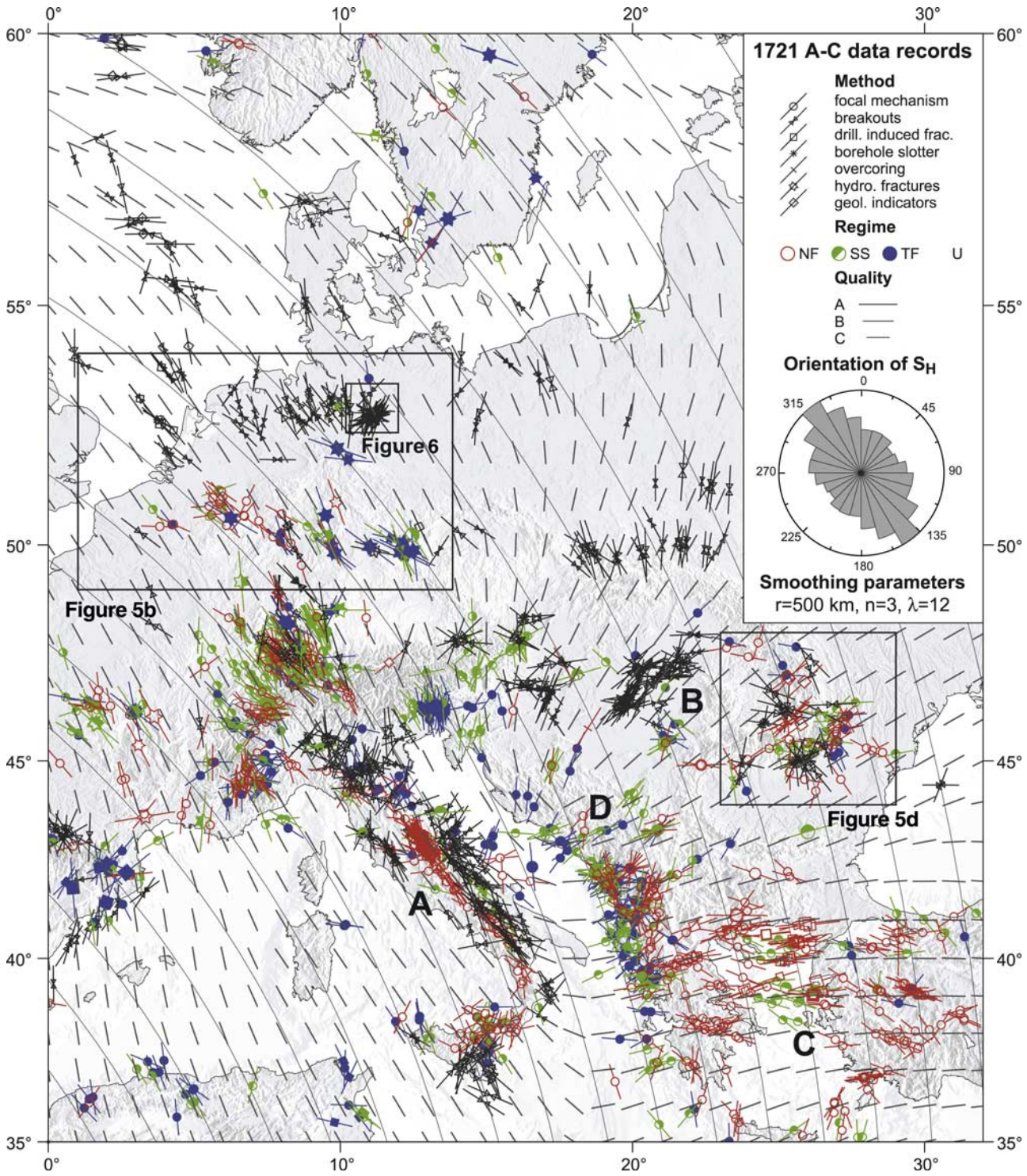

Figure 4. Stress map of western Europe. Stress symbols and smoothed stress field legend are as in Figure 1. Smoothing parameters are the search radius (r), the minimum number of data (n) within the search radius, and the smoothing factor (λ). Thin gray lines represent the relative plate motion trajectories of the Africa Plate with respect to the Eurasia Plate from the global plate model NUVEL-1A [*DeMets et al.*, 1990, 1994]. Topography is based on the ETOPO2 data from the National Geophysical Data Center (NGDC) including bathymetry data from *Smith and Sandwell* [1997]. Note the rose diagram showing that the prevailing S_H orientation is approximately 145°. Letters label the areas of Italy (A), the Pannonian Basin (B), Aegean and western Anatolia (C), and the Dinarides (D).

3.2. Regional-Scale Stress Patterns: Impact of Topography, Density, and Strength Contrasts

3.2.1. Stress Map of Northern Germany and Netherlands

[21] Close examination of the western European stress map (Figure 4) over northern Germany and Netherlands (Figure 5b) reveals more regional details of the stress pattern. Whilst the plate-scale stress field for this region indicates stresses to be NW-SE to NNW-SSE (Figure 4), zooming in on the same data set reveals a regional fan-shaped stress pattern with stresses ranging from NW-SE in the west to NE-SW in the east (Figure 5b). This fan-like stress pattern was noted for the first time by *Grünthal and Stromeyer* [1992]. Initially this observation was based on a very small data set, but more stress data provided by *Grünthal and Stromeyer* [1994] and *Roth and Fleckenstein* [2001] further supported the suggested fan-like stress pattern. Finally, this stress pattern was confirmed in the WSM 2005 database release owing to the addition of 298 data records in northern Germany and Netherlands, largely from borehole breakout analysis (Figure 5b). These data mainly came from WSM research projects in collaboration with the German Society for Petroleum and Coal Science and Technology, DGMK [*Fleckenstein et al.*, 2004], the Federal Office for Radiation Protection, BfS [n = 85, *Connolly et al.*, 2003], the Organization of Applied Natural Sciences in Holland, TNO [n = 97, *van Eijs and van Dalfsen*, 2004], and publications of *Grote* [1998] (n = 42) and *Roth and Fleckenstein* [2001] (n = 5).

[22] *Roth and Fleckenstein* [2001] discuss three possible reasons for this regionally differing trend in the eastern part of the North German Basin: (1) the influence of possible displacement along the Trans-European Suture Zone which separates the old East European platform from the younger western European parts of the Eurasia Plate, (2) the local dominance of stresses caused by postglacial rebound, and (3) the northward increase of lithospheric strength below the northeastern part of the North German Basin possibly acting as a barrier. The 2.5D finite element models support either the third hypothesis [*Marotta et al.*, 2002] or a combination of the first and third hypotheses [*Kaiser et al.*, 2005]. However, in both numerical approaches, the studied sections of the North German Basin are unfortunately close to their eastern model boundary, resulting in a high likelihood for modeling artifacts due to boundary effects in the easternmost parts of the basin.

[23] A potential fourth source of the stress field rotation in the North German Basin is the stresses induced by lateral density and strength contrasts across the Sorgenfrei-Teisseyre and Tornquist-Teisseyre zone where crustal thickness increases sharply from about 35 km in the west to 50 km in the East European platform [*Thybo*, 2001]. This increase in crustal thickness may produce enough gravitational potential energy to create compressional stresses perpendicular to the NW-SE striking suture zone. *Gölke and Coblentz* [1996] investigated the impact of the lateral density contrast due to topography in a large-scale 2D finite element model of western Europe and proved that these lateral density contrasts are likely to have an impact on the stress magnitudes, but only a small effect on stress orientations. *Jarosinski et al.* [2006] also included the effect of the varying lithospheric strength, as well as the effect of the topography, in their 2.5D finite element model of western Europe and reciprocated a swing of the stress field orientation in the eastern parts of the North German Basin, roughly in agreement with the observed stress. They also implemented the NW-SE striking Hamburg-Elbe fault zone as the southern boundary of the eastern section of the North German Basin. However, the faults in their model displays an unrealistic large displacement of 200–300 m in a predominantly aseismic area.

[24] In summary, the fan-shaped stress pattern in the North German Basin and farther east is now confirmed on a large, high-density stress data set, but the various processes contributing to this stress pattern are still controversial and have yet to be resolved. So far, the existing models reveal that mechanical and density contrasts, boundary conditions and geometry, as well as postglacial rebound contribute to a certain extent to the stress field reorientations across the North German Basin, but their relative importance is still questionable.

3.2.2. Stress Map of Venezuela

[25] Most of the 81 new data records come from a comprehensive compilation by *Colmenares and Zoback* [2003], and to a lesser extent, from publications of *Pérez et al.* [1997a, 1997b], *Taboada et al.* [2000], *Russo et al.* [1993], and from Harvard CMT solutions [e.g., *Ekström et al.*, 2003]. *Colmenares and Zoback* [2003] identified two distinct stress provinces in Venezuela, each with different S_H orientations. In eastern Venezuela, along the right-lateral El Pilar-Boconó transform fault, a strike-slip faulting stress regime prevails with a broadly NW-SE S_H orientation (Figure 5c). Farther west, toward the eastern Cordilleras,

Figure 5. Legend, stress symbols and smoothed stress field legend as in Figure 1a. (a) Stress map of Australia. Note the change of the regional stress in southeastern Australia. (b) Stress map of northern Germany and Netherlands. The mean S_H orientation of 144°N is in agreement with the direction of relative plate motion of approximately 137°N between the Africa Plate and the Eurasia Plate as previously observed by *Müller et al.* [1992]. However, note the deviation from this trend in the eastern part of the North German Basin where a rotation to NE is observed. Box indicates location of Figure 6. (c) Stress map of Venezuela. Note the difference in S_H orientation and stress regime in the eastern (NW-SE, strike-slip faulting) and the western part (W-E, thrust faulting) of Venezuela. EB denotes El Pilar-Boconó fault. (d) Stress map of Romania. Grey thick line indicates the location of a high-velocity body in the upper mantle at ~120 km depths according to the tomography study by *Martin et al.* [2005]. This body, a remnant of Miocene subduction, is sinking with ~2 cm/a vertically into the mantle and is in the state of slab break-off [*Sperner et al.*, 2001; *Wenzel et al.*, 1998].

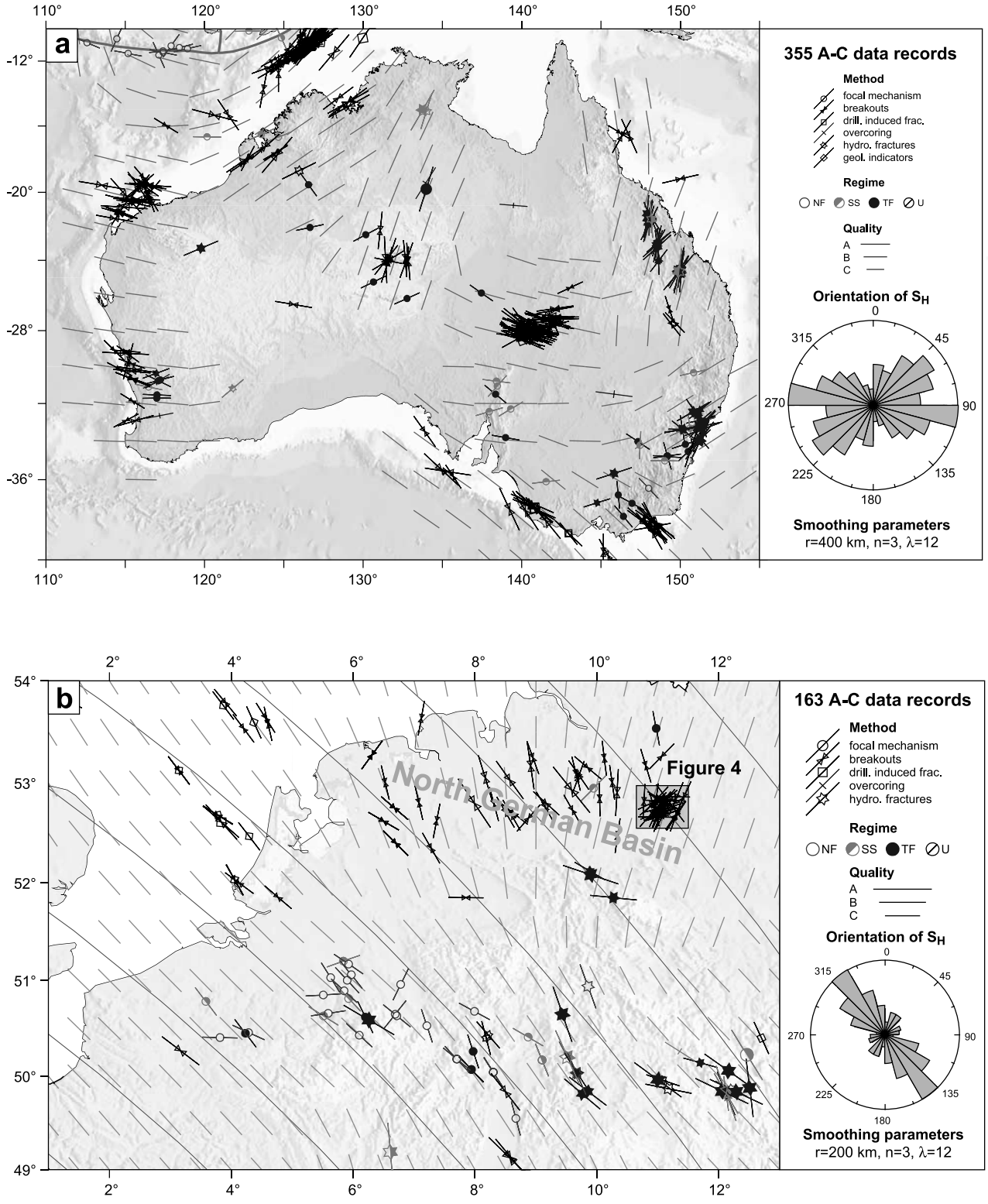
a
355 A-C data records
Method
focal mechanism
breakouts
drill. induced frac.
overcoring
hydro. fractures
geol. indicators
Regime
NF SS TF U
Quality
A
B
C
Orientation of S_H
0
45
90
135
180
225
270
315
Smoothing parameters
r=400 km, n=3, λ=12
110°
120°
130°
140°
150°
-12°
-20°
-28°
-36°
b
163 A-C data records
Figure 4
North German Basin
Smoothing parameters
r=200 km, n=3, λ=12
2°
4°
6°
8°
10°
12°
54°
53°
52°
51°
50°
49°

Figure 5

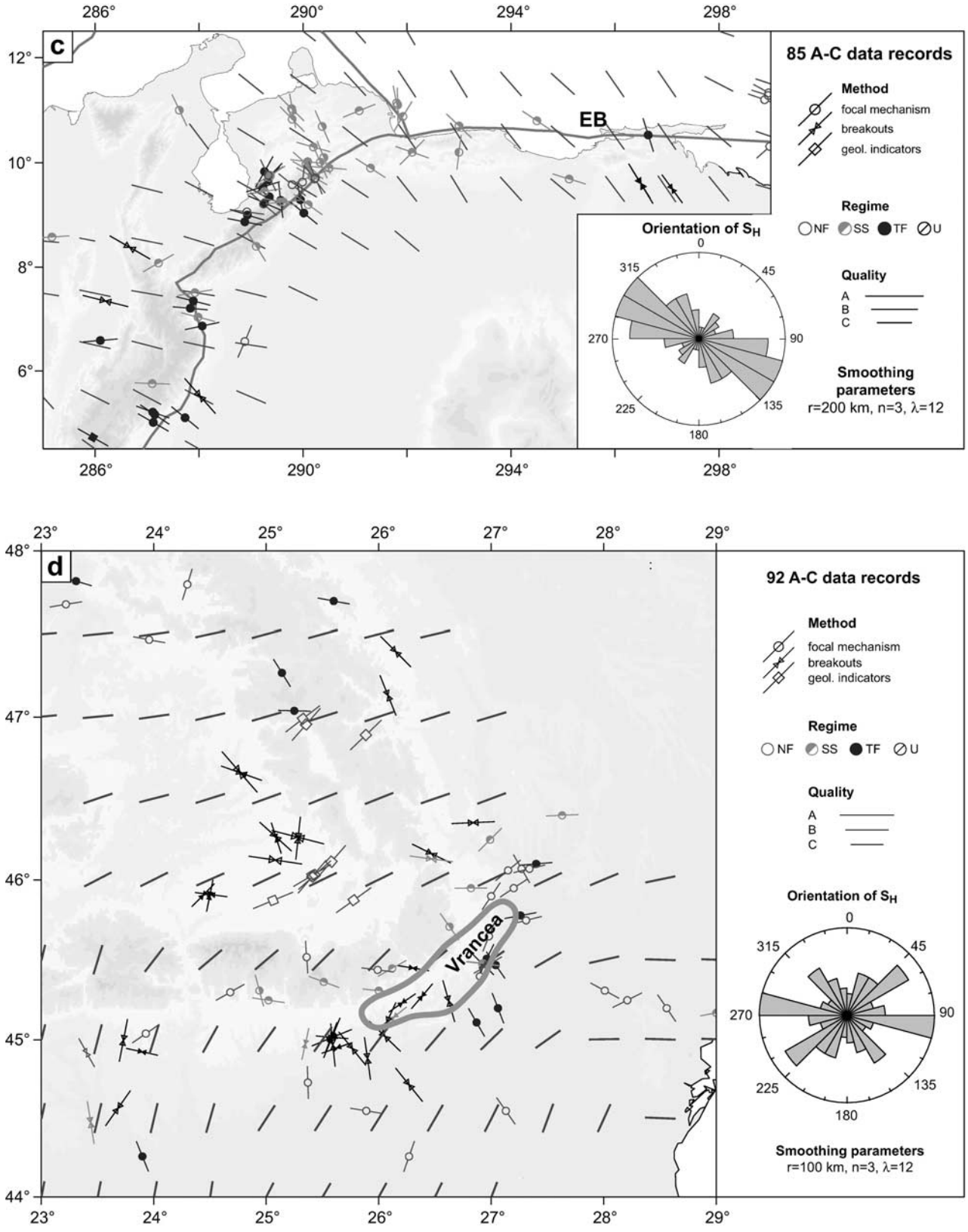

Figure 5. (continued)

the tectonic regime changes toward thrust faulting and the S_H orientation rotates anticlockwise following the regional trend of topography (Figure 5c). The latter, and to a lesser extent the former, indicates that areas with high topography store enough gravitational potential energy to be a second-order, regionally dominant, control on the tectonic regime and the S_H orientation. Indeed, the global WSM database reveals numerous areas in which stresses are largely perpendicular to mountain ranges, such as the Western Canada Basin, Papua New Guinea and around the Alps (Figure 1b). A consequence of this is that stresses in foreland basins, which are sparsely sampled in the 2005 WSM release, are likely to exhibit present-day stress patterns perpendicular to the topographic front.

3.2.3. Stress Map of Romania

[26] Recently the stress information in Romania and adjacent areas have been increased by 108 data records mainly provided by M. Negut and A. Negut (unpublished work from 2002 and 2004). Thus the total number of stress data records in Romania increased to 208, 92 of which have A-C quality. In contrast, the stress pattern presented by *Bada et al.* [1998], that indicates a homogeneous WNW-SES S_H orientation, the stress patterns from our new compilation do not show clear trends (Figure 5d). There are three possible explanations for this enigma: (1) The stress data set used by *Bada et al.* [1998] probably also included focal mechanism solutions from subcrustal earthquakes within the subducting slab at 70–130 km (whereas the WSM database only includes data within the upper 40 km of the earth). (2) The smoothing parameter applied by *Bada et al.* [1998] filtered only the first-order pattern on a plate-wide scale (e.g., a large search radius of 500 km as used in Figure 4 for the Eurasia Plate). (3) The smaller number of stress data records available at that time could not reveal the complicated local stress pattern.

[27] The high variability of S_H orientations in our stress map is most likely the result of relatively isotropic and/or low far-field horizontal stress magnitudes in the area. Such low or isotropic far-field stress magnitudes allow small local stress effects to control the in situ stress and thus result in a locally perturbed stress field. According to *Sonder* [1990], the net stress field as a superposition of local and regional stresses depends on the magnitudes of the regional principal stresses, the magnitudes of the local stress component as well as the angular difference of the regional principal stress directions to the stresses caused by the local stress source. Local additional stresses that are not parallel to the regional stresses will cause the net stress field to change the orientations of the principal stresses and can also change the faulting style from for example strike-slip faulting to normal faulting on local scales. Similar localized stress perturbations, thought to be due to low and/or isotropic horizontal stresses, are observed in the central and northern North Sea and Permian Basin [*Tingay et al.*, 2006].

[28] From the diversity of S_H orientations and the changes in the tectonic regime on short spatial scales in Romania (Figure 5d) we conclude that the contribution from plate boundary forces on the magnitude of tectonic stresses is small and that the stress tensor has similar eigenvalues, i.e., a stress state that is close to isotropic. This implies that third-order sources have a large influence on both the S_H orientation and the tectonic regime. Possible local stress sources are topography, lateral density and strength contrasts (Focsani Basin with 11 km depth, foreland, Mohesian platform), basin subsidence due to slab pull of a former subduction zone, and stress rotations at fault tips. Superposition of these different stress sources leads to a complex stress field with S_H orientations changing within a few kilometers.

[29] The high variation of the local stress pattern in Romania puts upper bounds to potential regional stress sources in the region such as the degree of coupling of the subducting Vrancea slab. We hypothesize that the slab beneath Vrancea does not transfer large amounts of stresses to the crust and that the coupling is probably weak. A strong coupling would produce a large regional signal in the stress pattern which cannot be identified in the stress observations. However, this hypothesis still needs to be investigated in detail with a 3D numerical model in order to compare the differential stresses produces by the local stress sources and the ones superimposed from different slab coupling scenarios.

3.3. Local-Scale Stress Patterns: Impact of Detachment Horizons

3.3.1. Eastern Part of the North German Basin

[30] High-resolution stress data sets from sedimentary basins indicate that stress orientations can locally deviate strongly from the regional stress field orientation. Detailed analysis of present-day stresses within sedimentary basins reveals significant and complex variations in the present-day S_H orientation [*Tingay et al.*, 2005b; *Tingay et al.*, 2006]. The eastern section of the North German Basin gives an excellent example for such a local-scale variation. Zooming into the cluster of data records in the eastern part of the North German Basin (Figure 6) reveals that two mean S_H orientations exist: An E-W orientation from stress data at shallow depth (1500–3300 m) above the Zechstein evaporite sequences and a SW-NE orientation from stress data at greater depth (3400–4500 m) reflecting the far-field orientation with the observed regional fan-shaped pattern. This vertically decoupled stress pattern in the eastern part of the North German Basin is not visible in its western and central parts where stress data above and below the Zechstein follow roughly the same regional trend.

[31] This large change of mean S_H orientation with depth is interpreted to be primarily the result of the Zechstein evaporites acting as a mechanically weak detachment layer, and therefore not enabling transmission of the regional stress field into shallower sequences. The detachment of regional stresses results in relatively isotropic horizontal stress magnitudes above the salt and thus allows small local stress sources to have a dominant influence on the stress pattern. Most likely the cause of the localized stress perturbations in the shallow detached sequences are the large density and strength contrasts provided by the numerous salt domes in this region [*Roth and Fleckenstein*, 2001]. Such decoupling horizons are not unusual for sedimentary basins

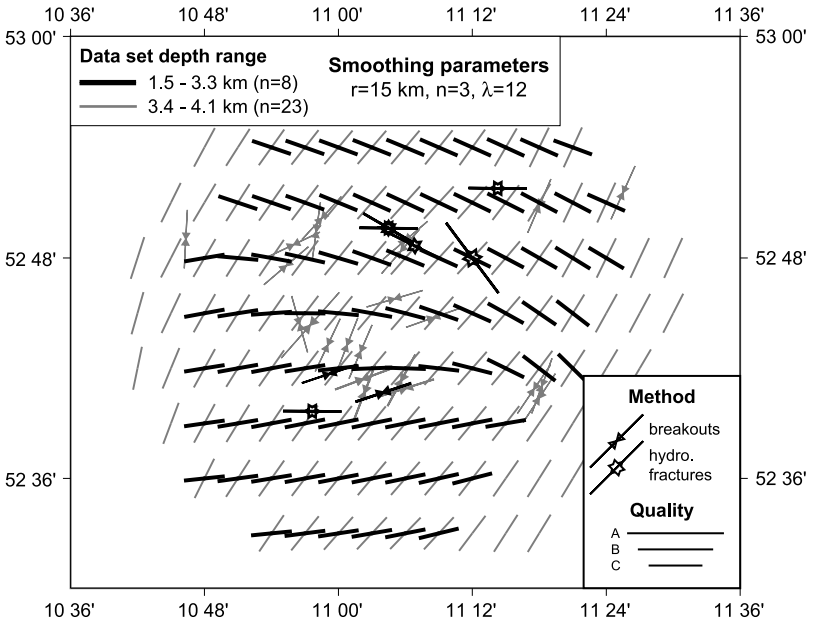

Figure 6. Stress map of the eastern part of the North German Basin. Stress symbols and smoothed stress field legend are as in Figure 1, and location is indicated in Figure 5b. The smoothed S_H orientations are calculated for two data sets from different depth ranges. Note the difference between the approximately E-W orientation in the upper layer (black symbols, 1.5–3.3 km, post-Zechstein) and the SW-NE orientation at greater depths (grey symbols, 3.4–4.1 km Zechstein) that reflects the regional stress field as displayed in Figure 5b.

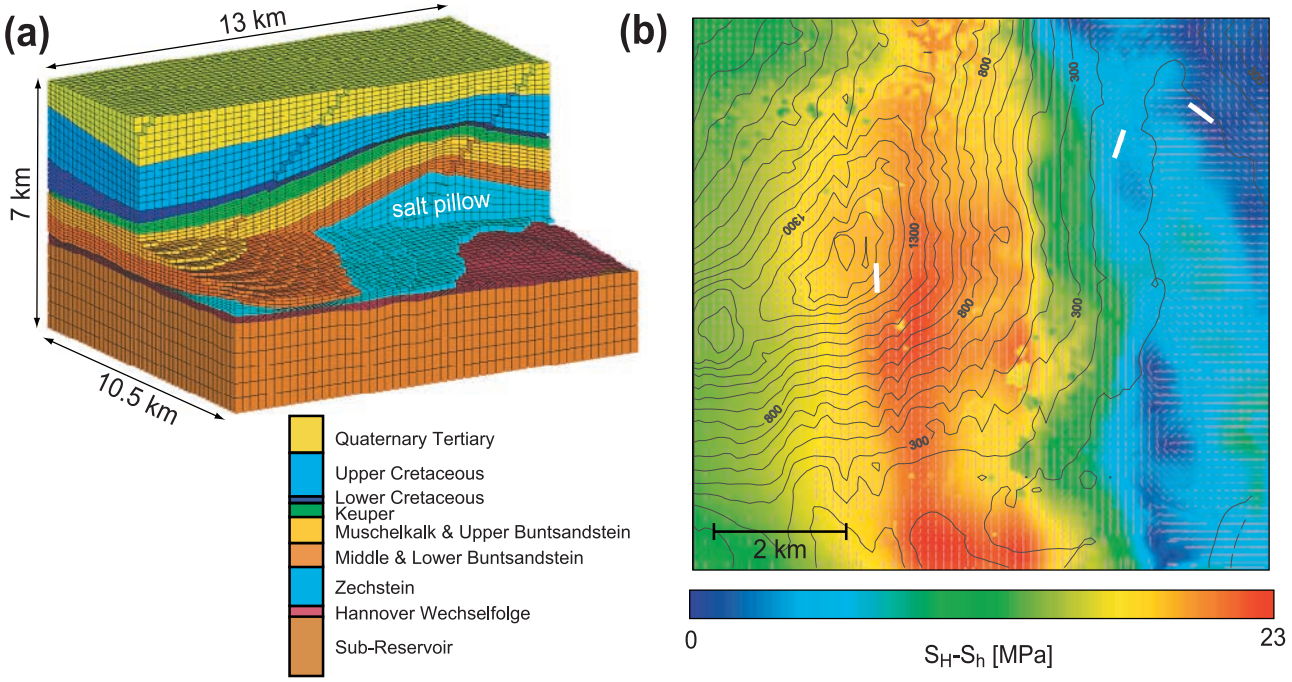

Figure 7. (a) Cutaway oblique view of the 3D finite element mesh with ~125,000 hexahedral linear elements. Model rheology is linear elastic, boundary conditions are a N-S oriented regional stress field and gravity. Density and mechanical rock properties vary according to the numbers given by *Fleckenstein et al.* [2004]. (b) Comparison of observed (white line symbols) and modeled (short red lines) S_H orientation at 4444 m depth (intra-Rotliegend) from the northern section of the finite element model. Grey contours are the Zechstein isopatches in meters; north is the vertical direction.

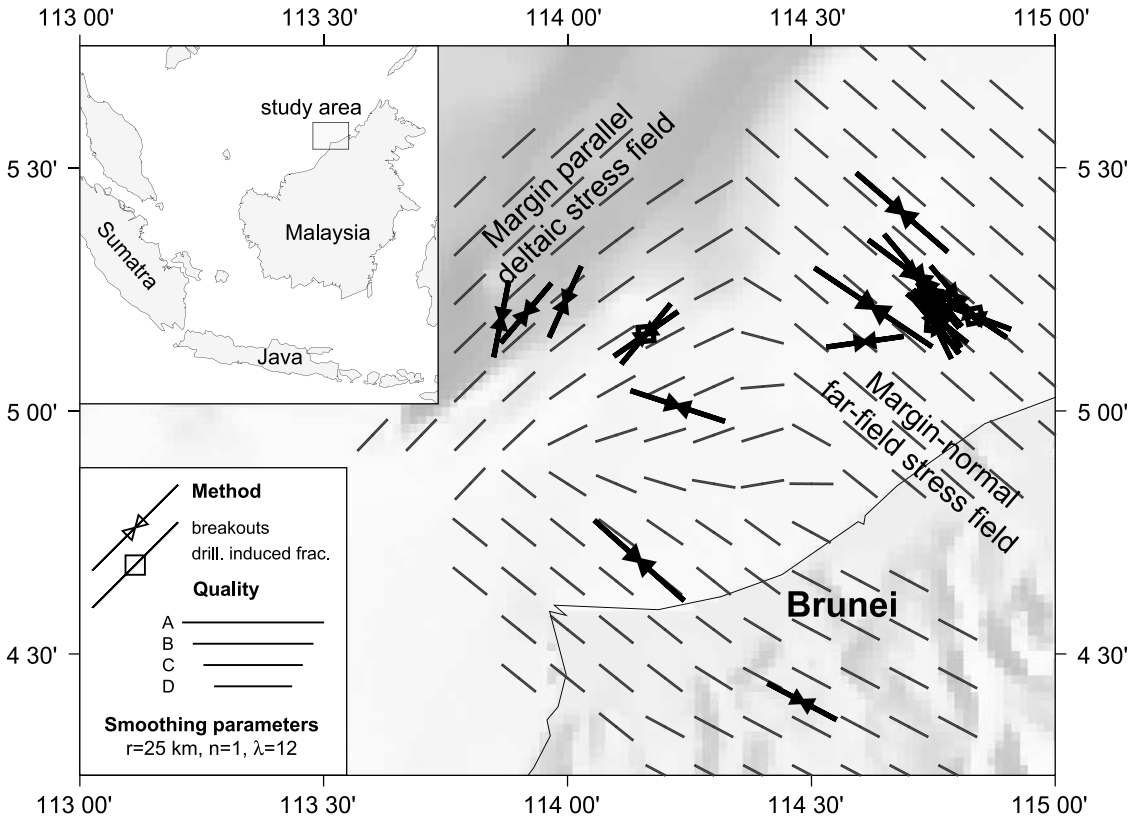

Figure 8. Stress map of the Baram Basin in Brunei. Stress symbols and smoothed stress field legend are as in Figure 1. Note the change of stress orientation offshore.

and are often visible where detailed analysis of present-day stresses reveal significant and complex variations in the present-day S_H orientation [*Tingay et al.*, 2005b]. Indeed, the Zechstein evaporite sequences are also believed to form a basal detachment and result in a similarly complex stress pattern in the central North Sea. The salt layer thickness in the North German Basin is highly variable and ranges from several hundred meters to a local thickness up to 4000 m due to halokinesis [*Scheck and Bayer*, 1999]. Measurements beside and above such salt pillows have a major impact on the stress orientations [*Brereton and Müller*, 1991].

[32] The influence of local density and mechanical contrasts in the vicinity of salt diapirs on the stress field has been demonstrated in 3D numerical experiments [*Fleckenstein et al.*, 2004]. The 3D finite element model geometry represents a existing salt pillow of up 1500 m thickness in the eastern part of the North German Basin (Figure 7a). Boundary conditions are gravitational forces and N-S compression due to the regional trend of the regional stress field. The impact of this salt layer structure is clearly seen in the model results at 4444 m depth (*c.* intra-Rotliegend) presented in Figure 7b. Differential stresses have magnitudes of up to 23 MPa and S_H rotates up to 80° on horizontal distances of less than one kilometer. The comparison with three data records from the WSM database (Figure 7b) shows that the model fits the large change in S_H orientation on small spatial scales very well.

[33] The eastern part of the North German Basin provides an excellent example of the local-scale third-order variations in the stress orientation that can be observed from petroleum industry data acquired in sedimentary basins. The systematic compilation of tectonic stresses from borehole data, which allows analysis of stress patterns at very small scales (0.1–100 km), reveals information that would never have been identified using seismicity data alone. The WSM 2005 database release contains information from ~70 sedimentary basins, enabling unique insights into the controls on stress changes in sedimentary basins. These changes result from the combination of various factors acting on different spatial scales, including far-field forces from the plate boundaries as well as more regional to local effects from basin geometry, geological structures, mechanical contrasts (e.g., evaporites, overpressured shales, detachment zones), topography and deglaciation [*Tingay et al.*, 2005b, 2006].

3.3.2. Stress Field of the Baram Delta Province of Brunei

[34] The Tertiary Baram Delta province of Brunei provides another excellent example of stress rotations resulting from local stress fields overprinting regional stress patterns. The early Miocene to present Baram Delta province is a series of three rapidly depositing and prograding delta sequences that were deposited adjacent to the NW Borneo active margin. The older and proximal (inboard) parts of the

Baram Delta province exhibit NW-SE stress orientations that are normal to the margin and are consistent with plate motion and the most recent (Pliocene to recent) NW-SE oriented inversion of structures in the inner shelf (Figure 8) [*Tingay et al.*, 2005a, 2003]. Hence this NW-SE inner shelf stress field is believed to be the result of far-field regional stresses exerted from either the plate boundaries, ongoing convergence of the continental salient with Borneo, delamination of the proto–South China Sea subducted slab, or from topographic forces caused by the Crocker-Rajang mountain range [*Tingay et al.*, 2005a]. However, in contrast to the regional NW-SE inner shelf stress field, a NE-SW (margin-parallel) stress field is observed in the outer shelf, near the shelf edge (Figure 8) [*Tingay et al.*, 2005a]. This margin-parallel NE-SW outer shelf stress field is consistent with active margin-parallel striking growth faulting and seabed scarps observed on bathymetry and shallow seismic data in this region (Figure 8) [*Tingay et al.*, 2005a]. The margin-parallel stresses observed in the outer shelf are consistent with a local "deltaic" stress field derived from gravitational instability of the convex-upward deltaic wedge. Hence the regional NW-SE S_H orientation in Brunei has been locally overprinted by a basally detached margin-parallel deltaic stress field. Furthermore, the primary original structures observed in the inner shelf are Miocene-Pliocene deltaic margin-parallel striking faults and folds that are inconsistent with the present-day margin-normal stress orientation. Hence the local spatial stress rotation observed in Brunei also reveals that stresses in the inner shelf of Brunei have rotated approximately 90° since the middle Miocene and that the region of NE-SW margin-parallel deltaic stresses has moved basinward over time (prograded), from the inner shelf to the present-day shelf edge [*Tingay et al.*, 2005a].

4. Change of Stress Pattern on Geological Timescales

[35] The examples in the previous chapter confirm that the stress pattern is mainly controlled by the superposition of tectonic forces acting along plate boundaries or arising from density contrasts including the effects of topography, mechanical rock properties, and active faults. However, the contemporary stress pattern is only the final stage of a long tectonic record that has to be taken into account to understand the geodynamic evolution of an area.

[36] Time-dependent effects on the stress pattern occur on timescales as short as earthquake cycles owing to tectonic loading, coseismic stress release, and postseismic stress relaxation [e.g., *Bohnhoff et al.*, 2006; *Freed and Lin*, 1998; *Hardebeck and Hauksson*, 2001; *Hergert and Heidbach*, 2006], but also on geological timescales on the order of millions of years, for example, as a result of changing plate boundary configurations and mountain growth [e.g., *Hippolyte et al.*, 1994; *Iaffaldano et al.*, 2006; *Lamb*, 2006; *Mercier et al.*, 1992; *Sandiford*, 2002; *Sandiford et al.*, 2004]. These time-dependent changes of the stress pattern can be studied by means of the geological record, paleostress analysis, paleomagnetic investigations or GPS and InSAR observations [*Barke et al.*, 2007; *Bertotti et al.*, 2001; *Delvaux et al.*, 1997; *Heidbach and Drewes*, 2003; *Melbourne et al.*, 2002; *Pritchard*, 2006; *Sandiford et al.*, 2004]. On the basis of these observations, it is possible to establish numerical models reflecting the geodynamic evolution and the contemporary stress pattern and tectonic regime at their final stage. In the following we present two examples to illuminate the advantage of combining stress data with geological information that enables us to investigate the geodynamic evolution and the relative importance of the forces causing the stress pattern through time.

4.1. Stress Field of Southeastern Australia

[37] *Sandiford et al.* [2004] combine stress data, numerical modeling, and the geological record in order to investigate the sources of stress manifested in the unusual stress pattern in southeastern Australia. They observe that the onset of faulting in southeastern Australia, that is still active under the present stress regime, correlates with the onset of the growth of the Southern Alps (New Zealand) in the late Miocene. The growth of the Southern Alps is due to the increase of convergence rate between the Indo-Australia Plate and the Pacific plate in the late Miocene from 2 mm/a to 10 mm/a [*Batt and Braun*, 1999] that is ongoing and reflected in GPS data at the transpressional Alpine Fault [*Beavan et al.*, 2002]. From numerical experiments *Sandiford et al.* [2004] concluded that the resulting increase of resistive forces at the plate boundary on the southern island of New Zealand generates the NW-SE trend of the S_H orientation. This indicates that the oceanic crust is capable to transfer stresses over thousands of kilometers between New Zealand and Australia and that even small changes in the plate boundary configuration have a significant impact on the S_H orientation.

4.2. Stress Field of Southern Italy

[38] The growth of the Apennines in Italy is the result of subduction processes in the central Mediterranean in Miocene and early Pliocene followed by continental collision in middle Pliocene and Pleistocene (Figure 9) [*Ziegler*, 1988; *Malinverno and Ryan*, 1986; *Mantovani et al.*, 1996; *Mueller and Kahle*, 1993]. According to *Hipployte et al.* [1994] this continental collision formed the Apennines in a ENE-WSW oriented compressional tectonic regime. However, the contemporary stress pattern in southern Italy and the Adriatic Block exhibits normal and strike-slip faulting regime (Figures 4 and 9) [*Montone et al.*, 2004; *Mariucci et al.*, 1999] with NW-SE S_H orientation parallel to the strike of the Apennines. This stress pattern is prevailing throughout southern Italy including the Apenninic foreland and foredeep, as well as the adjacent offshore of the Tyrrhenian Sea and the Adriatic Sea (Figure 9). *Hipployte et al.* [1994] concluded from the analysis of paleostress data that the stress pattern in southern Italy rotated significantly in early Pleistocene to middle Pleistocene and that the tectonic regime changed from compressional to normal faulting at that time. These changes indicate that new geodynamic processes commenced in middle Pleistocene and that these are ongoing.

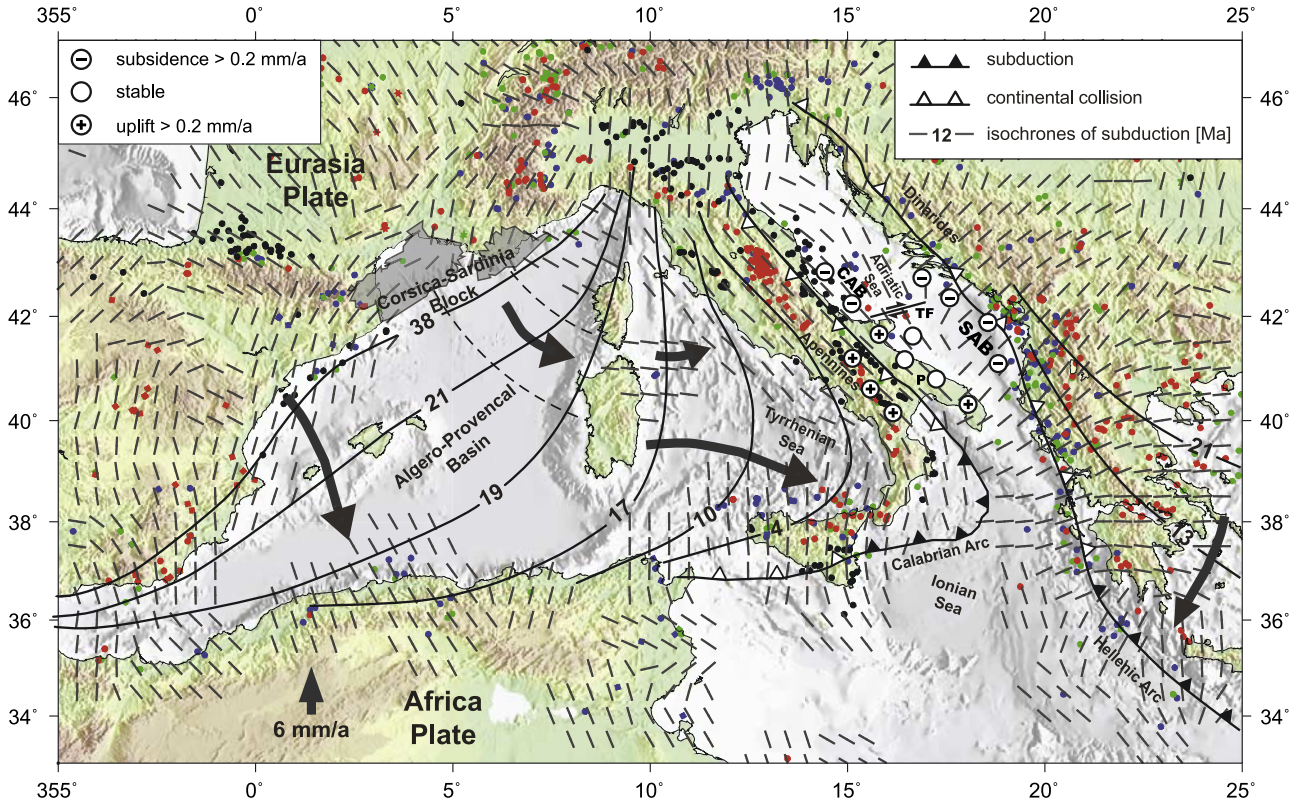

Figure 9. Geodynamic evolution and recent stress map of the western and central Mediterranean. Legend for stress symbols and smoothed stress field is as in Figure 1b. Abbreviations are: P, Puglia; CAB, Central Adriatic Basin; SAB, Southern Adriatic Basin; and TF, Tremiti Fault zone. Subsidence rates are taken from *Bertotti et al.* [2001]. Motion of the Africa Plate with respect to the Eurasia Plate is taken from NUVEL-1A [*DeMets et al.*, 1994]. Parameters for the smoothed stress field from A-C quality data are: r = 100 km, λ = 12, and n = 3. Isochrons display the SW migration of the subduction zone through time [*Mantovani et al.*, 1996; *Robertson and Grasso*, 1995; *Malinverno and Ryan*, 1986]. Back-arc spreading formed the Algero-Provençial basin that led to a 70° counterclockwise rotation of the Sardinia-Corsica Block [*Mueller and Kahle*, 1993]. On the eastern side of the Adriatic block, continental collision had already started in early Miocene to middle Miocene that gave rise to the Dinarides [*Ziegler*, 1988]. Note the focused and small section of subduction along the Calabrian Arc.

[39] *Hipployte et al.* [1994] hypothesize that these changes are due to slab break-off as suggested by seismic tomography [e.g., *Spakman*, 1990]. The expected vertical rebound caused by slab break-off is in agreement with the rapid uplift pattern in the Puglia region of southern Italy where Pleistocene sediments are found at 450–700 m height [*Bertotti et al.*, 2001; *Doglioni et al.*, 1994]. However, it contradicts the ongoing subsidence of the central Adriatic basin (Figure 9). *Doglioni et al.* [1994] explain the uplift pattern of Puglia with a steepening of the subducted lithosphere beyond Puglia leading to buckling of the lithosphere. In their model the subsidence of the central Adriatic basin decoupled to this process by the dextral Tremiti fault zone dividing the thick lithosphere (110 km) south of it from the thinner one (70 km) in the north (Figure 9). *Bertotti et al.* [2001] suggest that lithospheric folding (buckling) resulting from lateral compression is the cause of the observed uplift and subsidence pattern.

[40] Thus the contemporary stress field pattern in southern Italy is not reflecting the shortening from SW-NE compression of the Adriatic block as indicated by the tectonic record or the accretion of the Apennines, but it expresses a very recent geodynamic process of either slab break-off, slab steepening, or lithospheric folding. Even though the relative importance of these processes for the contemporary subsidence and stress pattern remains enigmatic this data integration gives new insights into geodynamic evolution of the region.

5. Conclusion and Perspectives of the WSM Database

[41] The WSM 2005 database release has developed regions of high data record density that enable us to investigate variations in stress orientations at local scales and to discuss sources controlling the third-order stress

Table 2. Sources of Crustal Stresses on Different Spatial Scales

Source	Examples	Effect on Stress Field	Length Scale
Plate boundary forces	ridge push, collision, subduction, mantle drag	*first-order control*	100 s to 1000 s of km
Large volume forces	mountain ranges, isostatic compensation, continent-ocean transition, Moho, lithosphere thickness variations, large basins	*second-order control* rotation of stress field due to mechanical and density contrasts between units	100 s of km
Flexural forces	deglaciation, subduction zones	*second-order control*	100 s of km
Detachment zones	evaporites, overpressured shales, low-angle faults	*second- to third-order control* changes mechanically overlying rocks from first- or second-order stress field	10 s to 100 s of km
Strong earthquakes	plate boundaries, major intraplate faults	*second- to third-order control* temporal changes linked to the seismic cycle	10 s to 100 s of km
Geological structures	faults, fractures, diapirs, folds	*third-order control* change due to mechanical and density contrasts between units	0.01 – 10 km

patterns. The stress patterns presented in the examples allow four major conclusions: (1) The plate-wide and regional stress pattern is controlled by the plate boundary forces confirming the findings from earlier work using the WSM database [e.g., *Hillis and Reynolds*, 2000; *Richardson*, 1992; *Coblentz and Richardson*, 1995; *Zoback*, 1992; *Zoback et al.*, 1989]. (2) The contemporary stress pattern in the WSM database reveals also third-order effects on small spatial scales. Zooming into the western European stress map (Figures 4, 5b, and 6), where data density is high, we identified areas where regional to local effects control the stress pattern at different spatial scales. (3) Additional stress sources are necessary (i.e., forces which are not related to plate boundaries) in order to explain regional- to local-scale stress patterns in regions where the contribution of plate boundary forces is small. In dependence of the stress magnitudes of the plate-wide-scale stress field regional and local stress sources can control the S_H orientation and the tectonic regime. The various stress sources and the spatial scales on which they are effective are summarized in Table 2. (4) The examples for the stress changes throughout geological times reveal that an integrated analysis of the WSM data with other information such as the geological record and the geodynamic evolution gives new insights into the relative importance of the sources of stress and their changes through geological times.

[42] This progress in understanding the contemporary stress pattern at different spatial scales has only been possible owing to the ongoing systematic compilation of stress data with international collaboration. For the forthcoming WSM database release we will focus on three issues: (1) The first issue is refinement of the quality assessments for focal mechanism solutions, borehole breakouts and hydraulic fractures. These changes are necessary owing to technical improvements and new methodologies that will be tested for their suitability as stress indicators (in comparison with the other methods). (2) The second issue is continuation of our worldwide initiative to intensify collaborations with the petroleum industry where most of the stress data in sedimentary basins are acquired. On the basis of the first results of this initiative we expect numerous new stress data records from areas with up-to-now low data coverage (e.g., Caspian Sea, SE-Asia, Nile delta). (3) The third issue is inclusion of new stress data records deduced from focal mechanism solutions using regional broadband data for waveform inversion. Focus of this work is on earthquakes with magnitudes lower than those used for the Global CMT Project (formally known as Harvard CMT catalogue) located in intraplate areas where sparse or no stress information is currently available.

[43] In spite of the numerous improvements and upgrades reported in this publication, the future success of the WSM is nevertheless dependent on the assistance of the scientific community and the ongoing support from our partners from industry. We thus call for active participation in the development of the next WSM database release regardless of which type of support: new stress data, the analysis of the stress field of a specific region, or discussions on new stress determination methods.

[44] **Acknowledgments.** The World Stress Map project is a collaborative project that would not be possible without the effort of many scientists worldwide. We are indebted to numerous individual researchers and working groups all over the world for providing stress data. The complete list of contributors is too numerous to be given herein. However, the authors are particularly grateful for major contributions for the WSM 2005 database release by Richard Hillis and Scott Reynolds of the Australasian Stress Map project (University of Adelaide), Lourdes Colmenares (Stanford University), Philip Fleckenstein (Karlsruhe University), Mihaela Negut (PETROM, Bucarest), Paola Montone (INGV, Rome), Maria Teresa Mariucci (INGV, Rome), Mark Zoback (Stanford University), and John Townend (University of Wellington). We also thank the World Stress Map advisory board members Egon Althaus, John Cook, Roy Gabrielsen, Domenico Giardini, Helmut Kipphan, Onno Oncken, Chris Reigber, Markus Rothacher, and Mark Zoback for their long-term and ongoing

support. We also thank the former members of the WSM research team Philipp Fleckenstein and Peter Connolly for providing us with the 3D FE example and very fruitful discussions on the stress pattern of the North German Basin. The manuscript has been greatly improved by encouraging and constructive reviews from Mike Sandiford, David Coblentz, and Kurt Stüwe.

References

Assumpção, M. (1992), The regional intraplate stress field in South America, *J. Geophys. Res.*, *97*(B8), 11,889–11,903.

Bada, G., S. Cloetingh, P. Gerner, and F. Horváth (1998), Sources of recent tectonic stress in the Pannonian region: Inferences from finite element modelling, *Geophys. J. Int.*, *134*, 87–101.

Bada, G., F. Horváth, P. Dövényi, P. Szafián, G. Windhoffer, and S. Cloetingh (2007), Present-day stress field and tectonic inversion in the Pannonian basin, *Global Planet. Change*, *58*, 165–180.

Barke, R., S. Lamb, and C. MacNiocaill (2007), Late Cenozoic bending of the Bolivian Andes: New paleomagnetic and kinematic constraints, *J. Geophys. Res.*, *112*, B01101, doi:10.1029/2006JB004372.

Batt, G. E., and J. Braun (1999), The tectonic evolution of the Southern Alps, New Zealand: Insights from fully thermally coupled dynamical modelling, *Geophys. J. Int.*, *136*, 403–420.

Beavan, J., P. Tregoning, M. Bevis, T. Kato, and C. Meertens (2002), Motion and rigidity of the Pacific Plate and implications for plate boundary deformation, *J. Geophys. Res.*, *107*(B10), 2261, doi:10.1029/2001JB000282.

Bell, J. S. (1996a), In situ stresses in sedimentary rocks (Part 2): Applications of stress measurements, *Geosci. Can.*, *23*, 135–153.

Bell, J. S. (1996b), In situ stresses in sedimentary rocks (Part 1): Measurement techniques, *Geosci. Can.*, *23*, 85–100.

Bertotti, G., V. Picotti, C. Chilovi, R. Fantoni, S. Merlini, and A. Mosconi (2001), Neogene to Quaternary sedimentary basins in the south Adriatic (Central Mediterranean): Foredeeps and lithospheric buckling, *Tectonics*, *20*(5), 771–787.

Bird, P. (2003), An updated digital model for plate boundaries, *Geochem. Geophys. Geosyst.*, *4*(3), 1027, doi:10.1029/2001GC000252.

Bird, P., Z. Ben-Avraham, G. Schubert, M. Andreoli, and G. Viola (2006), Patterns of stress and strain-rate in southern Africa, *J. Geophys. Res.*, *111*, B08402, doi:10.1029/2005JB003882.

Bohnhoff, M., H. Grosser, and G. Dresen (2006), Strain partitioning and stress rotation at the North Anatolian fault zone from aftershock focal mechanisms of the 1999 Izmit Mw = 7.4 earthquake, *Geophys. J. Int.*, *166*, 373–385.

Brereton, N. R., and B. Müller (1991), European stress: Contributions from borehole breakouts, in *Tectonic Stress in the Lithosphere*, edited by R. B. Whitmarsh et al., pp. 165–177, R. Soc., London.

Brudy, M., M. D. Zoback, F. Fuchs, F. Rummel, and J. Baumgärtner (1997), Estimation of the complete stress tensor to 8 km depth in the KTB scientific drill holes: Implications for crustal strength, *J. Geophys. Res.*, *102*(B8), 18,453–18,457.

Coblentz, D., and R. M. Richardson (1995), Statistical trends in the intraplate stress field, *J. Geophys. Res.*, *100*(B10), 20,245–20,255.

Coblentz, D., and R. M. Richardson (1996), Analysis of the South American intraplate stress field, *J. Geophys. Res.*, *101*(B4), 8643–8657.

Coblentz, D. D., and M. Sandiford (1994), Tectonic stresses in the African plate: Constraints on the ambient lithospheric stress state, *Geology*, *22*, 831–834.

Coblentz, D., S. Zhou, R. R. Hillis, R. M. Richardson, and M. Sandiford (1998), Topography, boundary forces, and the Indo-Australian intraplate stress field, *J. Geophys. Res.*, *103*(B1), 919–931.

Colmenares, L., and M. D. Zoback (2003), Stress field and seismotectonics of northern South America, *Geology*, *31*, 721–724.

Connolly, P., M. Gölke, H. Bäßler, P. Fleckenstein, S. Hettel, M. Lindenfeld, A. Schindler, U. Theune, and F. Wenzel (2003), Finite Elemente Modellrechnungen zur Erklärung der Auffächerung der größten horizontalen Hauptspannungsrichtung in Norddeutschland, *BfS Rep. Proj. Gorleben 9G2643110000*, 163 pp., Geophys. Inst., Univ. Karlsruhe, Karlsruhe, Germany.

Delvaux, D., R. Moeys, G. Stapel, C. Petit, K. Levi, A. Miroshnichenko, and V. Ruzhich (1997), Paleostress reconstructions and geodynamics of the Baikal region, Central Asia, Part 2. Cenozoic rifting, *Tectonophysics*, *282*, 1–38.

DeMets, C., R. G. Gordon, D. F. Argus, and S. Stein (1990), Current plate motions, *Geophys. J. Int.*, *101*, 425–478.

DeMets, C., R. G. Gordon, D. F. Argus, and S. Stein (1994), Effect of recent revisions to the geomagnetic reversal time scale on estimates of current plate motions, *Geophys. Res. Lett.*, *21*(20), 2191–2194.

Doglioni, C., F. Mongelli, and P. Pieri (1994), The Puglia uplift (SE Italy): An anomaly in the foreland of the Apenninic subduction due to the buckling of a thick continental lithosphere, *Tectonics*, *13*(5), 1309–1321.

Dyksterhuis, S., R. A. Albert, and R. D. Müller (2005), Finite-element modelling of contemporary and palaeointraplate stress using ABAQUS, *Comput. Geosci.*, *31*, 297–307.

Ekström, G., A. M. Dziewonski, N. N. Maternovskaya, and M. Nettles (2003), Global seismicity of 2001: Centroid-moment tensor solutions for 961 earthquakes, *Phys. Earth Planet. Inter.*, *136*, 165–185.

Ekström, G., M. Dziewonski, N. N. Maternovskaja, and M. Nettles (2005), Global seismicity of 2003: Centroid-moment-tensor solutions for 1087 earthquakes, *Phys. Earth Planet. Inter.*, *148*, 327–351.

Fleckenstein, P., G. Reuschke, B. Müller, and P. Connolly (2004), Predicting stress reorientations associated with major geological structures in sedimentary sequences, *DGMK Rep. 593-5*, 141 pp., Dtsch. Wiss. Ges. für Erdöl, Erdgas und Kohle, Celle, Germany.

Freed, A. M., and J. Lin (1998), Time-dependent changes in failure stress following thrust earthquakes, *J. Geophys. Res.*, *103*(B10), 24,393–24,409.

Fuchs, K., and B. Müller (2001), World Stress Map of the Earth: A key to tectonic processes and technological applications, *Naturwissenschaften*, *88*, 357–371.

Gölke, M., and D. Coblentz (1996), Origins of the European regional stress field, *Tectonophysics*, *266*, 11–24.

Grote, R. (1998), Die rezente horizontale Hauptspannungsrichtung im Rotliegenden und Oberkarbon in Norddeutschland, *Erdol Erdgas Kohle*, *114*, 478–483.

Grünthal, G., and D. Stromeyer (1992), The recent crustal stress field in central Europe: Trajectories and finite element modeling, *J. Geophys. Res.*, *97*(B8), 11,805–11,820.

Grünthal, G., and D. Stromeyer (1994), The recent crustal stress field in central Europe sensu lato and its quantitative modelling, *Geol. Mijnbouw*, *73*, 173–180.

Hardebeck, J. L., and E. Hauksson (2001), Crustal stress field in southern California and its implications for fault mechanics, *J. Geophys. Res.*, *106*(B10), 21,859–21,882.

Hardebeck, J. L., and A. J. Michael (2004), Stress orientations at intermediate angels to the San Andreas Fault, California,, *J. Geophys. Res.*, *109*, B11303, doi:10.1029/2004JB003239.

Harris, R. A. (2002), Stress triggers, stress shadows and seismic hazard, in *International Handbook of Earthquake and Engineering Seismology*, *Int. Geophys. Ser.*, vol. 81B, edited by W. H. K. Lee et al., pp. 1217-1231, Academic Press, Amsterdam.

Harris, R. A., R. W. Simpson, and P. A. Reasenberg (1995), Influence of static stress changes on earthquake locations in southern California, *Nature*, *375*, 221–224.

Heidbach, O., and Z. Ben-Avraham (2007), Stress evolution and seismic hazard of the Dead Sea fault system, *Earth Planet. Sci. Lett.*, *257*, 299–312.

Heidbach, O., and H. Drewes (2003), 3-D finite element model of major tectonic processes in the Eastern Mediterranean, in *New Insights in Structural Interpretation and Modelling*, *Spec. Publ. Ser.*, vol. 212, edited by D. Nieuwland, pp. 259–272, Geol. Soc., London.

Heidbach, O., and J. Höhne (2007), CASMI—A tool for the visualization of the World Stress Map database, *Comput. Geosci.*, in press.

Heidbach, O., A. Barth, P. Connolly, F. Fuchs, B. Müller, J. Reinecker, B. Sperner, M. Tingay, and F. Wenzel (2004), Stress maps in a minute: The 2004 World Stress Map release, *Eos Trans. American Geophysical Union*, *85*, 521–529.

Heidbach, O., K. Fuchs, B. Müller, J. Reinecker, B. Sperner, M. Tingay, and F. Wenzel (2007), The World Stress Map—Release 2005, map, 1:46,000,000, Comm. of the Geol. Map of the World, Paris.

Hergert, T., and O. Heidbach (2006), New insights in the mechanism of postseismic stress relaxation exemplified by the June 23rd 2001 Mw = 8.4 earthquake in southern Peru, *Geophys. Res. Lett.*, *33*, L02307, doi:10.1029/2005GL024858.

Hillis, R. R., and S. D. Reynolds (2000), The Australian Stress Map, *J. Geol. Soc.*, *157*, 915–921.

Hillis, R. R., S. D. Mildren, C. J. Pigram, and D. R. Willoughby (1997), Rotation of horizontal stresses in the Australian North West continental shelf due to the collision of the Indo-Australian and Eurasian plates, *Tectonics*, *16*(2), 323–335.

Hillis, R. R., J. R. Enever, and S. D. Reynolds (1999), In situ stress field of eastern Australia, *Aust. J. Earth Sci.*, *46*, 813–825.

Hippolyte, J.-C., J. Anglier, and F. Roure (1994), A major geodynamic change revealed by Quatenary stress patterns in the Southern Appenines (Italy), *Tectonophysics*, *230*, 199–210.

Humphreys, E. D., and D. D. Coblentz (2007), North American dynamics and western U. S. tectonics, *Rev. Geophys.*, *45*, RG3001, doi:10.1029/2005RG000181.

Iaffaldano, G., H.-P. Bunge, and T. Dixon (2006), Feedback between mountain belt growth and plate convergence, *Geology*, *34*, 893–896, doi:10.1130/G22661.1.

Jarosinski, M., F. Beekman, G. Bada, and S. Cloetingh (2006), Redistribution of recent collision push and ridge push in Central Europe: Insights from FEM modelling, *Geophys. J. Int.*, *167*, 860–880.

Kaiser, A., K. Reicherter, C. Hübscher, and D. Gajewski (2005), Variation of the present-day stress field within the North German Basin—Insights from thin shell FE modeling based on residual GPS velocities, *Tectonophysics*, *397*, 55–72.

King, G. C. P., R. S. Stein, and J. Lin (1994), Static stress changes and the triggering of earthquakes, *Bull. Seismol. Soc. Am.*, *84*, 935–953.

Lamb, S. (2006), Shear stresses on megathrusts: Implications for mountain building behind subduction zones, *J. Geophys. Res.*, *111*, B07401, doi:10.1029/2005JB003916.

Ljunggren, C., Y. Chang, T. Janson, and R. Christiansson (2003), An overview of rock stress measurement methods, *Int. J. Rock Mech. Min. Sci.*, *40*, 975–989.

Malinverno, A., and W. B. F. Ryan (1986), Extension in the Tyrrhenian Sea and shortening in the Apennines as result of arc migration driven by sinking of the lithosphere, *Tectonics*, *5*, 227–245.

Mann, P., and A. Taira (2004), Global significance of the Solomon Islands and Ontong Java Plateau convergence zone, *Tectonophysics*, *389*, 137–190.

Mantovani, E., D. Albarello, C. Tamburelli, and D. Babbucci (1996), Evolution of the Tyrrhenian basin and surrounding regions as a result of the Africa-Eurasia convergence, *J. Geodyn.*, *21*, 35–72.

Mariucci, M. T., A. Amato, and P. Montone (1999), Recent tectonic evolution and present stress in the Northern Apennines (Italy), *Tectonics*, *18*, 108–118.

Marotta, A. M., U. Bayer, H. Thybo, and M. Scheck (2002), Origin of the regional stress in the North German basin: Results from numerical modelling, *Tectonophysics*, *360*, 245–264.

Martin, M., and F. Wenzel (2005), High-resolution teleseismic body wave tomography beneath SE-Romania—II. Imaging of a slab detachment scenario, *Geophys. J. Int.*, *164*, 579–595.

Meijer, P. T., and M. J. R. Wortel (1992), The dynamics of motion of the South American Plate, *J. Geophys. Res.*, *97*(B8), 11,915–11,931.

Meijer, P. T., R. Govers, and M. J. R. Wortel (1997), Forces controlling the present-day state of stress in the Andes, *Earth Planet. Sci. Lett.*, *148*, 157–170.

Melbourne, T. I., F. H. Webb, J. M. Stock, and C. Reigber (2002), Rapid postseismic transients in subduction zones from continuous GPS, *J. Geophys. Res.*, *107*(B10), 2241, doi:10.1029/2001JB000555.

Mercier, J. L., M. Sebrier, A. Lavenu, J. Cabrera, O. Bellier, J.-F. Dumont, and J. Machare (1992), Changes in the tectonic regime above a subduction zone of Andean type: The Andes of Peru and Bolivia during the Pliocene-Pleistocene, *J. Geophys. Res.*, *97*(B8), 11,945–11,982.

Montone, P., M. T. Mariucci, S. Pondrelli, and A. Amato (2004), An improved stress map for Italy and surrounding regions (central Mediterranean), *J. Geophys. Res.*, *109*, B10410, doi:10.1029/2003JB002703.

Mueller, S., and H.-G. Kahle (1993), Crust-mantle evolution, structure and dynamics of the Mediterranean-Alpine region, in *Contribution of Space Geodesy to Geodynamics: Crustal Dynamics*, *Geodyn. Ser.*, vol. 23, edited by D. E. Smith and D. L. Turcotte, pp. 249–298, AGU, Washington, D. C.

Müller, B., M. L. Zoback, K. Fuchs, L. Mastin, S. Gregersen, N. Pavoni, O. Stephansson, and C. Ljunggren (1992), Regional patterns of tectonic stress in Europe, *J. Geophys. Res.*, *97*(B8), 11,783–11,803.

Müller, B., V. Wehrle, S. Hettel, B. Sperner, and F. Fuchs (2003), A new method for smoothing oriented data and its application to stress data, in *Fracture and In-Situ Stress Characterization of Hydrocarbon Reservoirs*, *Spec. Publ. Ser.*, vol. 209, edited by M. Ameen, pp. 107–126, Geol. Soc., London.

Nalbant, S. S., J. McCloskey, S. Steacy, and A. A. Barka (2002), Stress accumulation and increased seismic risk in eastern Turkey, *Earth Planet. Sci. Lett.*, *195*, 291–298.

Pérez, O. J., M. A. Jaimes, and E. Garciacaro (1997a), Microseismicity evidence for subduction of the Caribbean Plate beneath the South American Plate in northwestern Venezuela, *J. Geophys. Res.*, *102*(B8), 17,875–17,882.

Pérez, O. J., C. Sanz, and G. Lagos (1997b), Microseismicity, tectonics and seismic potential in southern Caribbean and northern Venezuela, *J. Seismol.*, *1*, 15–28.

Pritchard, M. E. (2006), InSAR, a tool for measuring Earth's surface deformation, *Phys. Today*, *59*, 68–69.

Provost, A.-S., and H. Houston (2003), Stress orientations in northern and central California: Evidence of the evolution of frictional strength along the San Andreas plate boundary system, *J. Geophys. Res.*, *108*(B3), 2175, doi:10.1029/2001JB001123.

Reynolds, S. D., and R. R. Hillis (2000), The in situ stress field of the Perth Basin, Australia, *Geophys. Res. Lett.*, *27*(20), 3421–3424.

Reynolds, S. D., D. Coblentz, and R. R. Hillis (2002), Tectonic forces controlling the regional intraplate stress field in continental Australia: Results from new finite element modelling, *J. Geophys. Res.*, *107*(B7), 2131, doi:10.1029/2001JB000408.

Richardson, R. M. (1992), Ridge forces, absolute plate motions, and the intraplate stress field, *J. Geophys. Res.*, *97*(B8), 11,739–11,748.

Richardson, R. M., and L. M. Reding (1991), North American plate dynamics, *J. Geophys. Res.*, *96*(B7), 12,201–12,223.

Robertson, A. H. F., and M. Grasso (1995), Overview of the Late Tertiary-Recent tectonic and palaeo-environmental development of the Mediterranean region, *Terra Nova*, *7*, 114–127.

Roth, F., and P. Fleckenstein (2001), Stress orientations found in north-east Germany differ from the west European trend, *Terra Nova*, *13*, 286–289.

Russo, R. M., R. C. Speed, E. A. Okal, J. B. Shepherd, and K. C. Rowley (1993), Seismicity and tectonics of the southeastern Caribbean, *J. Geophys. Res.*, *98*(B8), 14,229–14,319.

Sandiford, M. (2002). Neotectonics of southeastern Australia: Linking the Quatenary faulting record with seismicity and in situ stress, in *Evolution and Dynamics of the Australian Plate*, edited by R. R. Hillis and D. Müller, *Spec. Publ. Geol. Soc. Aust.*, 22, 101-113.

Sandiford, M., M. Wallace, and D. Coblentz (2004), Origin of the in situ stress field in south-eastern Australia, *Basin Res.*, *16*, 325–338, doi:10111/j.1365-2117.2004.00235.x.

Scheck, M., and U. Bayer (1999), Evolution of the Northeast German Basin—Interferences from a 3D structural model and subsidence analysis, *Tectonophysics*, *313*, 145–169.

Smith, W. H. F., and D. T. Sandwell (1997), Global sea floor topography from satellite altimetry and ship depth soundings, *Science*, *277*, 1956–1962.

Sonder, L. (1990), Effects of density contrasts on the orientation of stresses in the lithosphere: Relation to principal stress directions in the Transverse ranges, California, *Tectonics*, *9*(4), 761–771.

Spakman, W. (1990), Tomographic images of the upper mantle below central Europe and the Mediterranean, *Terra Nova*, *2*, 542–553.

Sperner, B., F. Lorenz, K. Bonjer, S. Hettel, B. Müller, and F. Wenzel (2001), Slab break-off—Abrupt cut or gradual detachment? New insights form the Vrancea Region (SE Carpathians Romania), *Terra Nova*, *13*, 172–179.

Sperner, B., B. Müller, O. Heidbach, D. Delvaux, J. Reinecker, and K. Fuchs (2003), Tectonic stress in the Earth's crust: Advances in the World Stress Map project, in *New Insights in Structural Interpretation and Modelling*, edited by D. A. Nieuwland, *Geol. Soc. Spec. Publ.*, 212, pp. 101-116.

Steacy, S., J. Gomberg, and M. Cocco (2005), Introduction to special section: Stress transfer, earthquake triggering, and time-dependent seismic hazard, *J. Geophys. Res.*, *110*, B05S01, doi:10.1029/2005JB003692.

Stein, R. S., A. A. Barka, and J. H. Dietrich (1997), Progressive failure on the North Anatolian fault since 1939 by earthquake stress triggering, *Geophys. J. Int.*, *128*, 594–604.

Taboada, A., L. A. Rivera, A. Fuenzalida, A. Cisternas, H. Philip, H. Bijward, J. Olaya, and C. Rivera (2000), Geodynamics of the northern Andes: Subductions and intracontinental deformation (Colombia), *Tectonics*, *19*(5), 787–813.

Thybo, H. (2001), Crustal structure along the EGT profile across the Tornquist Fan interpreted from seismic, gravity and magnetic data, *Tectonophysics*, *334*, 155–190.

Tingay, M. R. P., R. R. Hillis, C. K. Morley, R. E. Swarbrick, and E. C. Okpere (2003), Variation in vertical stress in the Baram Basin, Brunei: Tectonic and geomechanical implications, *Mar. Pet. Geol.*, *20*, 1202–1212.

Tingay, M., R. R. Hillis, C. K. Morley, E. Swarbrick, and S. J. Drake (2005a), Present-day stress orientation in Brunei: A snapshot of 'prograding tectonic' in a Tertiary delta, *J. Geol. Soc.*, *162*, 39–49.

Tingay, M., B. Müller, J. Reinecker, O. Heidbach, F. Wenzel, and P. Fleckenstein (2005b), The World Stress Map Project 'Present-day Stress in Sedimentary Basins' initiative: Building a valuable public resource to understand tectonic stress in the oil patch, *Leading Edge*, *24*, 1276–1282.

Tingay, M. R. P., B. Müller, J. Reinecker, and O. Heidbach (2006), State and origin of the present-day stress field in sedimentary basins: New results from the World Stress Map Project, paper presented at Golden Rocks 2006, The 41st U. S. Symposium on Rock Mechanics (USRMS): 50 Years of Rock Mechanics—Landmarks and Future Challenges, Am. Rock Mech. Assoc., Golden, Colo.

Townend, J., and M. D. Zoback (2006), Stress, strain, and mountain-building in central Japan, *J. Geophys. Res.*, *111*, B03411, doi:10.1029/2005JB003759.

van Eijs, R., and W. van Dalfsen (2004), Borehole observations of maximum horizontal stress orientations in the Dutch upper crust, report, Geol. Surv. of the Netherlands (TNO-NITG), Utrecht, Netherlands.

Wagner, D., B. Müller, and M. Tingay (2004), Correcting for tool decentralisation of oriented 6-arm caliper logs for determination of contemporary tectonic stress orientation, *Petrophysics*, *46*, 530–539.

Wenzel, F., U. Achauer, E. Enescu, E. Kissling, R. Russo, V. Mocanu, and G. Musacchio (1998), Detailed look at final stage of plate break-off is target of study in Romania, *Eos Trans. AGU*, *79*, 589–594.

Wessel, P., and W. H. F. Smith (1998), New, improved version of Generic Mapping Tools released, *Eos Trans. AGU*, *79*, 579.

Ziegler, P. A. (1988), Evolution of the Arctic-North Atlantic and the Western Tethys, *AAPG Mem., 43*, 198 pp.

Zoback, M. D., and M. L. Zoback (1991), Tectonic stress field of North America and relative plate motions, in *Neotectonics of North America, Decade Map vol.I*, edited by D. B. Slemmons et al., pp. 339–366, Geol. Soc. of Am., Boulder, Colo.

Zoback, M. D., and M. L. Zoback (2002), State of stress in the Earth's lithosphere, in *International Handbook of Earthquake and Engineering Seismology*, *Int. Geophys. Ser.*, edited by W. H. K. Lee, P. C. Jennings, and H. Kanamori, pp. 559–568, Academic Press, Amsterdam.

Zoback, M. L. (1992), First- and second-order patterns of stress in the lithosphere: The World Stress Map project, *J. Geophys. Res.*, *97*(B8), 11,703–11,728.

Zoback, M. L., and K. Burke (1993), Lithospheric stress patterns: A global view, *Eos Trans. AGU*, *74*, 609–618.

Zoback, M. L., and W. D. Mooney (2003), Lithospheric bouyancy and continental intraplate stresses, *Int. Geol. Rev.*, *45*, 95–118.

Zoback, M. L., and M. D. Zoback (1989), Tectonic stress field of the conterminous United States, in Geophysical Framework of the Continental United States, edited by L. C. Pakiser and W. D. Mooney, *Mem. Geol. Soc. Am.* 172, 523-539.

Zoback, M. L., et al. (1989), Global patterns of tectonic stress, *Nature*, *341*, 291–298.

K. Fuchs, O. Heidbach, and F. Wenzel, Geophysical Institute, Karlsruhe University, Hertzstr. 16, 76187 Karlsruhe, Germany. (oliver.heidbach@gpi.uni-karlsruhe.de)

B. Müller, Heidelberg Academy of Sciences and Humanities, Karlstraße 4, D-69117 Heidelberg, Germany.

J. Reinecker, Institute of Geosciences, University of Tübingen, Sigwartstraße 10, D-72076 Tübingen, Germany.

B. Sperner, Geological Institute, TU Bergakademie Freiberg, Bernhard-von-Cotta-Straße 2, D-09599 Freiberg, Germany.

M. Tingay, School of Earth and Environmental Sciences, DP313 Mawson Building, University of Adelaide, Adelaide, SA 5005, Australia.